An assessment of the mantle and slab components in the magmas of an oceanic arc volcano: Raoul Volcano, Kermadec arc

Ian E M Smith[a,*], Richard C Price[b], Robert B Stewart[c], T J Worthington[a]

[a]*Geology Programme, School of Geography, Geology, and Environmental Sciences, University of Auckland, PB92019, Auckland 1142, New Zealand*
[b] *School of Science and Engineering, University of Waikato,PB3105, Hamilton , New Zealand*
[c] *Institute of Natural Resources, Massey university, PB11222, Palmerston North 4442, New Zealand*

Abstract

Raoul Volcano occupies a simple oceanic subduction setting in the northern part of the Kermadec Arc on the Pacific-Australian convergent plate boundary. The primary inputs to the magmatic system that feeds the volcano are a subduction component derived from the subducting old Pacific oceanic lithosphere and its veneer of pelagic sediment, and the overlying peridotitic mantle wedge. Conservative trace elements that are very incompatible during mantle melting are relatively depleted in Raoul lavas indicating a source that has been depleted during an earlier melting event. Major element co-variations indicate magma genesis by 25% near fractional melting of a mantle source that is weakly depleted (2% melt extraction) relative to a fertile MORB source. An important influence on the composition of the mantle component is progressive melt extraction coupled with minimal advection of fresh material into the sub-arc zone followed by melt extraction from a melting column beneath the spreading centre of an adjacent back arc basin. High field strength element and rare earth element systematics indicate involvement of a subduction-related component of constant composition. Two fluid components can be distinguished, one enriched in large ion lithophile elements inferred to be an aqueous fluid that is continuously added to the ascending melt column and the other a less mobile fluid that transfers Th. A homogeneous subduction-related component of constant composition and magnitude

arises if the slab-derived flux migrates from the slab-mantle interface to the sub-arc melting column by repeated episodes of amphibole formation and decomposition its composition is then governed by the distribution coefficients of pyroxene and its magnitude by the degree of amphibole saturation of mantle peridotite. The results from Raoul Volcano are comparable to those from other oceanic subduction-related arcs such as South Sandwich and Marianas suggesting that this is a general model for oceanic arcs.

Keywords: Kermadec arc, oceanic arcs, subduction zones, magma genesis.

* Corresponding Author. Geology Programme, School of Geography, Geology, and Environmental Sciences, University of Auckland, PB92019, Auckland 1142, New Zealand
Tel: +649 373 7599x87416
FAX: +649 373 7435
E-mail address: ie.smith@auckland.ac.nz

1. Introduction

Subduction related magmas are complex materials made up of components derived from multiple sources and assembled by a variety of processes. In currently popular models the components and processes involved in the formation of a typical arc-type magma include a contribution from the subducting slab, transfer of this component to the overlying mantle wedge, melting in the wedge to produce a primitive magma and profound modification of these primitive melts by crystallization, fractionation, melt mixing and assembly of the final product (e.g. Price et al., 2005; Eichelberger et al., 2006). Subduction-related magmas are characterized by their enrichment in large-ion lithophile elements (LILE) and depletion of high-field strength elements (HFSE) relative to mid-ocean ridge basalts (MORB) (e.g.Gill 1981; Pearce, 1983). Conventional models of subduction related magma genesis link these attributes to the transfer of a hydrous LILE - bearing HFSE depleted component from the subducting slab to the overlying mantle (e.g. Tatsumi et al., 1986; McCulloch and Gamble, 1991; Pearce and Peate, 1995).

In terms of chemical mass balance in subduction related magmatic systems, elements are termed conservative if they are not represented in the slab component and slightly (<40%), moderately (40-80%) or highly (>80%) non-conservative as their contribution from the slab increases relative to the mantle component (Pearce and Peate, 1995). The distinction between conservative and non-conservative elements is thus determined by transfer across the interface between the subducting slab and the mantle wedge. Potentially, the slab-derived component may be modified en route from the slab to the sub-arc melt generation zone by scavenging of some elements, loss of other elements, or by isotopic exchange (Navon and Stolper, 1987; Hawkesworth et al., 1991; Stolper and Newman, 1994; Pearce and Peate, 1995).

Both the subducted oceanic lithosphere and its overlying sediment veneer are potential sources of the slab derived component. Aqueous fluids generated in the slab have high LILE/HFSE ratios (e.g. Brenan et al., 1995; Keppler, 1996) and migrate across the mantle wedge in time scales of the order of 30-50 ka (Turner et al., 1996; 1997; Elliot et al., 1997). There is also evidence for a component which migrates on much shorter timescales (Davies, 1999; Handley et al., 2008; Caulfield et al., 2008). Conversely silicic melts derived from subducting sediment may bear both LILE and HFSE (McDermott et al., 1993; Nichols et al., 1994). Such melts probably leave the slab at shallower depths and may reside in the mantle wedge for several Ma before reaching the sub-arc melt generation zone (Turner and Hawkesworth, 1997).

Raoul Volcano (29°14'50" S 177°55'07" W) is located in a particularly simple part of the Tonga Kermadec arc (Fig.1) in what is arguably one of the simplest subduction settings on Earth. Raoul is the only volcano in the Kermadec Arc that has significant subaerial exposure and the lava sequences exposed on the island represent the longest documented time span (~10^4-10^5 years) and the greatest known variety of rock types of any Kermadec volcano. Raoul Island is small (maximum dimensions of 10 by 7 km, total area 29.4 km^2) but is the summit portion of a much larger volcanic massif that rises 900 m from the crest of the Kermadec Ridge and has a volume of 214 km^3. Raoul Volcano is located in the Northern Kermadec arc segment (Smith and Price, 2006) where the volcanoes rise from a relatively shallow Kermadec Ridge. In this segment there is minimal sediment subducting beneath the arc and there is no continental component to this. Therefore erupted magmas should contain a chemical signature free from continental input.

In this paper we use geochemical data from a suite of basaltic and andesitic lavas from Raoul Island to assess the relative roles of the different components and

processes that have contributed to the magmatic system that built the volcano. The data set on which the paper is based comprises a subset of samples that are representative of a larger database of 200 lava samples for which major and trace element analyses analysed by X-Ray Fluorescence are available. These representative samples have been analysed for minor trace elements and isotope ratios by ICP-MS and thermal ionization mass spectrometry (Table 1).

Most Raoul lavas are moderately to strongly porphyritic, some contain up to 48% phenocrysts (typically 20-30%) and a minority are sparsely phyric to aphyric with < 5% phenocrysts. All have a simple anhydrous mineral assemblage dominated by plagioclase accompanied by lesser amounts of clinopyroxene and minor olivine, orthopyroxene and spinel. Hornblende is not found in any Raoul lava although it does occur in xenoliths. The sparsely phyritic and aphyric samples comprise a relatively small group ranging from basalt to andesite. Silicic lavas are a subordinate but nonetheless significant component of the Raoul suite but as they have been effectively modelled as the products of crustal melting (Smith et.al., 2006) they are not relevant to this assessment of the sub-crustal processes and components beneath an oceanic arc.

Porphyritic samples show a variety of disequilibrium petrographic features that indicate that they are mixtures of silicate liquid and entrained crystals rather than crystallisation products of melts, and this includes basaltic and basaltic andesite compositions that have relatively high Mg# (Fig 2). The aphyric samples are interpreted to represent magmatic liquids but their compositions are clearly geochemically evolved. In this study we have placed emphasis on their chemical compositions as a means of assessing the inputs of the system as a whole while

acknowledging that they are the fractionated products of a primitive arc magma that is not represented in the exposed rocks of the volcano.

2. Assessing the mantle contribution

In the sense that the origin of arc-type magmas is in the mantle wedge above the subducting slab, the behavior of conservative elements in a subduction environment is directly comparable with that beneath oceanic spreading centers. Flat MORB normalized HFSE abundance patterns and low MORB normalized HFSE values (<1) typical of most low-SiO_2 subduction-related lavas indicate that these elements are conservative and that the degree of mantle melting beneath volcanic arcs exceeds that beneath spreading centres (eg Ewart and Hawkesworth, 1987; Pearce and Parkinson, 1993). However, some subduction-related lavas have negative anomalies for particular HFSE and others have positive anomalies. Variations also occur in the ratios of conservative elements such as Ta/Yb, Nb/Zr. Zr/Ti, Y/Sc and Ti/V. Both the frequency and magnitude of these deviations from MORB-like values mimic a sequence of decreasing distribution coefficient during melting of a spinel lherzolite source. This dependence on conservative element distribution coefficient (D_C) suggests that co-variations are sensitive indicators of mantle depletion or enrichment events (Ewart and Hawkesworth, 1987; McCulloch and Gamble, 1991; Pearce and Parkinson, 1993; Woodhead et al., 1993). These observations are consistent with recent work in the Tongan Arc where strongly sub-chondritic Nb/Ta ratios point to the involvement of a highly depleted source (Caulfield et al., 2008).

Fig. 3 illustrates the co-variations in Raoul lavas with respect to a fertile MORB mantle (FMM) source composition. The FMM-normalised pattern of Raoul lavas is comparable to that of average MORB for most moderately incompatible conservative

157 elements. Significantly, elements that are more incompatible than Y have lower
158 FMM-normalised abundances than those of MORB and this trend increases in
159 magnitude as D_C decreases. This is in spite of the fact that Raoul lavas are chemically
160 evolved. The relative depletion in elements such as Co, Mg, Cr and Ni can be
161 explained by their evolved chemistry.
162 Element ratios in which a conservative element is the numerator and another with
163 higher D_C is the denominator are consistently less for average MORB and vice-versa.
164 For example Ti/V in an average aphyric Raoul lava with <55wt% SiO_2 is 13
165 compared with 25 for MORB whereas Ti/Zr in aphyric Raoul lava is 129 compared
166 with 103 for MORB. Similar FMM-normalised trends and conservative element ratios
167 have been attributed to re-melting of a MORB-source mantle from which a small melt
168 fraction has been removed, the earlier event being responsible for depletion in highly
169 incompatible elements (Gamble et al., 1993; Pearce and Parkinson, 1993; Woodhead
170 et al., 1993).
171 A difference from the MORB pattern is a positive V_{FMM} anomaly in aphyric
172 Raoul lavas. This may reflect melting under more oxidizing conditions because the
173 oxidation state of V is sensitive to fO_2 and there is a marked difference between $D_{V(5+)}$
174 (~0.05) and $D_{V(3+)}$ (~5) for mantle melting, with the speciation of V changing rapidly
175 near the QFM buffer (Shevais, 1982; Carmichael and Ghiorso, 1990).
176 The sub-arc mantle beneath Raoul Volcano has the geochemical and geothermal
177 characteristics of a Pacific MORB source (Ewart and Hawkesworth, 1987; Hergt and
178 Hawkesworth, 1994; Pearce et al., 2007). The sub-arc mantle may also be mildly
179 depleted in incompatible elements relative to a fertile MORB mantle source. This
180 situation can be explained if mantle that had melted to generate new crust in the
181 northern Havre Trough was subsequently advected into the sub-arc region (e.g. Ewart

and Hawkesworth, 1987, Caulfield et al., 2008). Replenishment of the sub-arc mantle source can also occur by advection because of mechanical coupling at the slab-wedge interface where mantle adjacent to the descending slab is dragged down and a compensatory trench-ward flow is established in the overlying asthenosphere (e.g. Davies and Stevenson, 1992; Caulfield et al, 2008).

Most Raoul lavas have MgO < 6 wt.%, Mg# < 55, and none have the geochemical characteristics expected of primitive magma. Instead, they have undergone modification by fractional crystallization and crystal accumulation. One technique for removing the effects of fractional crystallization involves fitting regression lines for each element to MgO, and then extrapolating the element abundance to an MgO content of interest, typically 8 or 9 wt.% (here, Ca_8 will be used to refer to the CaO content extrapolated to MgO = 8.0 wt.%, etc). Although lavas with 8-9 wt. % MgO do not represent primary magmas, this extrapolation does provide a common reference point for the comparison of different magmatic suites and has been used with some success in studies of MORB and continental flood basalt petrogenesis (e.g., Klein and Langmuir, 1989; Turner and Hawkesworth, 1995). This style of regression also removes some of the effects of crustal contamination if that is coupled with fractionation. The technique assumes that the fractionating assemblage is of constant composition throughout the range of the extrapolation, and that the analyses on which the regression equations are based represent magmas. The major element composition of Raoul lavas were recalculated for MgO = 8 wt.% by linear regression (Table 2). The linear regression equations were calculated using only the group of aphyric lavas to derive equations that were then applied to all lavas with <57 wt.% SiO_2.

In the absence of a terrigenous sedimentary component CaO and Al_2O_3 are conservative during subduction-related magma genesis, although this may reflect

masking of any subduction-related component by the relatively high concentration of these elements in the mantle (e.g., Pearce and Parkinson, 1993). Strongly depleted mantle has lower $CaO/A1_2O_3$ values than normal mantle because $D_{Ca} < D_{Al}$ during melting. Therefore, magma generated by melting of depleted mantle is expected to have CaO/Al_2O_3 <0.75, which is the MORB value at MgO = 7.5 wt.% (Pearce and Parkinson, 1993). For the regressed Raoul lavas, Ca_8/Al_8 varies from 0.69-0.88 and averages 0.80. The high Ca_8/Al_8 values of Raoul lavas are not artefacts of plagioclase accumulation because if the dataset is restricted only to aphyric lavas the ratio actually increases to an average of 0.85. Both elements were therefore unaffected (or equally affected) by the depletion event indicated by low Nb_{FMM}, Zr_{FMM}, and Ti_{FMM} (Fig. 4).

Melting of depleted mantle is also expected to generate melts with higher Al_8/Ti_8 and Ca_8/Ti_8 than fertile mantle, as $D_{Ti} < D_{Al}$ and $D_{Ti} < D_{Ca}$. The regressed Raoul analyses form a linear trend with positive slope on a plot of $A1_8/Ti_8$ versus Ca_8/Ti_8 (Fig. 4). Aphyric lavas have Al_8 and Ca_8 equivalent to that of MORB at MgO = 7.5 wt.% (calculated from Pearce and Parkinson, 1993), whereas porphyritic lavas extend towards and into the field representing experimental melts from a depleted mantle source. The effect of crystal accumulation on the regressed analyses was modeled by adding plagioclase (An_{87}), clinopyroxene ($En_{46}Fs_{15}Wo_{39}$) and olivine (Fo_{70}) to an aphyric lava, and then calculating Al_8/Ti_8 and Ca_8/Ti_6. Vectors representing the addition of these phases are depicted on Fig. 4, and demonstrate that the trend of increasing Al_8/Ti_8 and Ca_8/Ti_8 from aphyric lavas through the range of porphyritic lavas is primarily an artefact of plagioclase accumulation. Other Kermadec lavas have significantly higher Al_8/Ti_8 and Ca_8/Ti_8 than Raoul aphyric lavas (Fig. 3). The Kermadec array overlaps that for strongly plagioclase-phyric Raoul lavas on Figure 4.

232 In summary, evidence for a depleted (relative to MORB) mantle source
233 beneath Raoul comes from low values of Nb_{FMM}, Zr_{FMM}, and Ti_{FMM}. The degree of
234 depletion is too small to affect elements of greater D_C during melt extraction, such as
235 Ca and Al and their concentrations in the sub-arc mantle are comparable to those in
236 normal MORB source mantle.

237

238 *2.1 Melting in the mantle wedge*

239 In widely accepted models, subduction-related magmas are linked to fluxing
240 by a hydrous component transferred from the subducting slab (e.g., Tatsumi et al.,
241 1986; Davies and Bickle, 1991; McCulloch and Gamble, 1991; Davies and Stevenson,
242 1992; Pearce and Peate, 1995). The fluid (or melt) derived from the slab reacts with
243 peridotite in the overlying mantle wedge to form amphibole, and this component is
244 progressively transferred to hotter regions of the mantle wedge by a complex cycle
245 involving amphibole decomposition at higher pressure and amphibole formation at
246 shallower depth. This cyclical process is limited by the amphibole-saturated peridotite
247 solidus (3.0 GPa, 1150 °C); above this, peridotite is too hot for new amphibole to
248 form and the mantle-melt mix ascends as a melting column. As the column rises
249 further melting is due to decompression, analogous to processes believed to occur
250 beneath spreading centers (Pearce and Parkinson, 1993). Note however, that although
251 this model is generally consistent with theoretical constraints the actual transfer
252 process of a hydrous fluid from the subducting slab is likely to be complex and multi-
253 staged (c.f. Davies 1999).

254 Theoretical and experimental studies of decompression melting beneath
255 spreading centers have led to the development of near-fractional melting models

256 (O'Hara, 1985 McKenzie and Bickle, 1988; Klein and Langmuir, 1987; 1989; Kinzler
257 and Grove, 1992). In this process, small melt fractions (~1 %) segregate from the
258 rising melting column, do not equilibrate with overlying mantle, and are aggregated at
259 shallower depth. Earlier melts from deeper in the melting column are enriched in
260 incompatible elements, whereas later melts from the higher, more depleted, column
261 are less enriched in these elements. Inefficient melt pooling produces aggregate
262 magmas with a range of compositions, each reflecting the average composition of its
263 amalgamated melts.

264 The co-variation of Na_8 and Fe_8 in MORB provides further insight into mantle
265 melting processes (Klein and Langmuir, 1987; 1989). Sodium is highly incompatible
266 during melting of spinel lherzolite as $D_{Na} \sim D_{Zr}$ (Sun and McDonough, 1989) and its
267 concentration in the melt decreases as the extent of melting increases. The Fe content
268 of a mantle melt increases with pressure and so the global Na_8 - Fe_8 array for MORB
269 has a negative slope (Fig. 5). High Na_8 - low Fe_8 lavas erupt at deep spreading centers
270 where the mantle temperature is inferred to be cool and the melting column short.
271 Conversely, low Na_8 - high Fe_8 lavas erupt at shallow spreading centers where the
272 mantle is inferred to be hottest and the melting column longest. Their geochemistry
273 indicates a large degree of melting at a greater average depth.

274 Raoul aphyric lavas plot on an extrapolation of the global MORB Na_8 - Fe_8
275 array to lower Na_8 and higher Fe_8 (Fig. 5). The low Na_8 - high Fe_8 end of the MORB
276 array can be generated by approximately 18 % total melting at an average pressure of
277 1.5 GPa (Kinzler and Grove, 1992). By analogy, the data for Raoul suggest a longer
278 mantle melting column that begins to melt at greater depth and undergoes more
279 melting. Although the earlier mantle depletion event indicated by low values of
280 Nb_{FMM}, Zr_{FMM}, and Ti_{FMM} in Raoul lavas will have reduced the Na content of the

mantle source, Fe_8 should not be affected by that event. If the Na content of aphyric lavas includes a significant subduction-related component, then the Na content of the mantle-derived component must be even lower than that indicated on Fig. 5. A conclusion from these data is that the low Na_8 and high Fe_8 values of Raoul lava are best explained by a greater degree of mantle melting than is generally the case beneath any spreading centre. Most porphyritic suite lavas from Raoul form a diffuse array with slightly positive slope, extending from the aphyric lavas toward lower Na_8 and Fe_8 values. The effect of crystal accumulation on Na_8 and Fe_8, shown as vectors on Fig.5 is modeled by adding plagioclase (An_{87}) clinopyroxene ($En_{46}Fs_{15}Wo_{39}$) and olivine (Fo_{70}) to an aphyric lava.

Lavas from other Tonga-Kermadec volcanoes have lower Fe_8 coupled with either comparable Na_8 (Tonga) or higher Na_8 (Kermadec). The higher Na_8 and lower Fe_8 may indicate less melting at a shallower average depth than that beneath Raoul. Conversely, the similar Na_8 but lower Fe_8 would suggest comparable degrees of melting at shallower depth. Further evidence of a high degree of melting beneath Raoul can be found in the abundances of conservative elements. Both Nb and Yb are highly incompatible during melting of spinel lherzolite, with $D_{Nb} < D_{Yb}$ (Sun and McDonough, 1989). In consequence, Nb/Yb is a sensitive measure of mantle melting and depletion because melt extraction will deplete Nb relative to Yb (Pearce and Parkinson, 1993). Nb abundance is plotted against Yb content in Fig. 6. Values of Nb and Yb in representative aphyric and porphyritic suite lavas have been regressed to MgO = 9 wt.% using the procedure outlined earlier and the higher value of MgO. 9 wt.% versus 8 wt.% was chosen for consistency with the calibration of the Nb_9 - Yb_9 array (Pearce and Parkinson, 1993).

Most of the Raoul lavas form a cluster in Nb_9 -Yb_9 space (Fig. 6). If the diagram is correctly calibrated, then they were generated by 15-35 % melting of a mantle source ranging in composition from FMM to a source depleted by 4 % melt extraction relative to FMM. An average Raoul lava would be generated by 25 % melting of a source depleted by 2 % melt extraction relative to FMM. This is broadly consistent with the evidence of >18 % melting from Na (Fig. 6). The Nb_9 / Yb_9 ratio is not sensitive to the effects of phenocryst contamination, and aphyric and porphyritic suite lavas overlap. However, if Nb (or possibly Yb) are contributed from a sedimentary component it follows that the wedge had a lower Nb and Yb content at 9% MgO which would infer greater degrees of depletion and larger amounts of melting.

Analyses from other intra-oceanic arcs yield comparable results (Pearce and Parkinson, 1993; Pearce et al., 1995; Peate et al., 1997). South Sandwich lavas require a slightly more depleted source and higher degree of melting, Mariana lavas require slightly less melting of a less depleted source, and New Hebrides lavas require slightly more melting of an FMM source (Fig.6). In contrast, lavas from continental margin arcs and those lacking active backarc extension (e.g., the Aleutians) have lower degrees of melting of mantle enriched relative to FMM.

3. Assessing the Subduction-Related Component

Although, the composition of the subduction-related component in Raoul lavas can be appraised in a general way from a MORB-normalised plot (Fig 7) detailed evaluation rests on the assumption that mantle melting beneath the volcano is analogous to that taking place beneath spreading centers. Theoretical studies and conservative element systematics in subduction-related lavas suggest that this assumption is valid, at least for a small volume hydrous flux (Pearce and Parkinson,

330 1993). Quantifying the magnitude of the subduction-related component for each
331 element is then dependent on seeing through the combined effects of near-fractional
332 melting, inefficient melt pooling to form aggregate magmas, polybaric open-system
333 fractional crystallisation, and late-stage crystal accumulation.

334 We have approached the problem by using the co-variation of incompatible
335 element abundances and Nb/Yb ratios (Pearce, 1983; Pearce et al., 1995; Pearce and
336 Peate, 1995). The conceptual basis for this approach is that Nb/Yb is highly sensitive
337 to near-fractional melting, melt pooling, and previous mantle depletion or enrichment
338 events, chiefly because $D_{Nb} < D_{Yb}$ during melting of spinel lherzolite (Sun and
339 McDonough, 1989) and so plotting other elements or element ratios against Nb/Yb
340 effectively normalizes them for variations in these parameters. Two assumptions are
341 inherent in this approach. Firstly that both Nb and Yb are conservative elements, and
342 neither is present in the subduction-related component for Raoul lavas, values of
343 Nb_{FMM} less than MORB and Yb_{FMM} equivalent to MORB provide strong evidence that
344 this is so (Fig. 3). Secondly, that both Nb and Yb are equally affected by fractional
345 crystallization or crystal accumulation. This is a good approximation, because $D_{Nb} \sim$
346 D_{Yb} for plagioclase, olivine, and pyroxene, and both are very small.

347 MORB-normalised plots of the form X/Yb versus Nb/Yb, (where X is an
348 incompatible element) produce an array of positive slope (i.e., increasing X/Yb with
349 increasing Nb/Yb) centered on the average MORB composition (Pearce and Peate,
350 1995). The array is interpreted as an artefact of the melting process. Early melts from
351 deep in the melting column have high X/Yb and Nb/Yb, whereas later melts from
352 higher in the now depleted column have lower X/Yb and Nb/Yb. This reflects the
353 situation where $D_X < D_{Yb}$ and $D_{Nb} < D_{Yb}$ during mantle melting. A negative array
354 slope would develop for $D_X > D_{Yb}$ The range of X/Yb and Nb/Yb in melts is partly

355 preserved in MORB because pooling to form aggregate magmas is inefficient, and not
356 all melts are represented by any one aggregate magma.

357 For subduction-related lavas, the equivalent plots should return the mantle
358 array if X is a conservative incompatible element. If X is a non-conservative
359 incompatible element, the slope and location of the array depends upon the
360 composition of the mantle, the subduction-related component, and how they are
361 mixed prior to melting.

362 Four distinct trends explain the behavior of non-conservative incompatible
363 elements in subduction zones and these are illustrated in Fig.8. Variable X/Yb at
364 constant Nb/Yb (trend A) results from the addition of a variable subduction-related
365 component to a mantle of constant composition. Near-fractional melting introduces
366 scatter parallel to the MORB array for both X/Yb and Nb/Yb, generating a rectangular
367 array centred along line A. Nearly constant X/Yb but variable Nb/Yb (trend B) arises
368 from the addition of a constant subduction-related component to a variable mantle
369 composition. Near-fractional melting enhances the spread in Nb/Yb and displaces
370 X/Yb values in directions parallel to the MORB array, leading to a rectangular array
371 centered on line B. A trend parallel to the MORB array but offset to higher X/Yb and
372 lower Nb/Yb (trend C) is best explained by a combination of events involving melt
373 extraction which generates a depleted mantle of constant composition (Cm) together
374 with a subduction-related component of constant composition added to the depleted
375 mantle to produce composition C at the end of the vertical open-headed arrow. Near-
376 fractional melting of the mix then generates the trend parallel to the MORB array.
377 Trends lying at an angle to the MORB array, along which SiO_2 increases from one
378 end (Dl) to the other (D2) are best explained as a Type C array (here offset to an
379 enriched mantle source) accompanied by progressive late-stage assimilation of crustal

material. Contour lines (dashed) representing the proportion of element X derived from the subduction-related component are parallel to the MORB array on these plots

We have assessed the proportion of each incompatible element contributed by the subduction related component in Raoul lavas using a series of X/Yb versus Nb/Yb plots (Fig.9). Plots of Zr/Yb and Ba/Yb versus Nb/Yb highlight the contrasting behavior of conservative and highly non conservative elements during subduction-related magma genesis. All Raoul lavas have Nb/Yb < average MORB, reflecting their derivation from a depleted mantle source as discussed above. They form an array that overlaps and scatters about the depleted MORB array on the Zr/Yb versus Nb/Yb plot, consistent with no subduction-related contribution of Zr. In contrast, on the Ba/Yb versus Nb/Yb plot they form an array parallel to that of MORB and offset to far higher Ba/Yb. This is a Type C array (Fig. 8), and contouring indicates that 96-98 % of Ba in these lavas is contributed by the subduction-related component.

Also plotted on Fig. 9 are compositional fields from the intra oceanic South Sandwich and Mariana arcs. South Sandwich database consists of 1-4 analyses from each of 12 different volcanoes (Pearce et al., 1995), and the Mariana database consists of 1-7 analyses from each of 7 different volcanoes (Elliott et a1., 1997). Both represent overview studies of entire arcs rather than detailed studies of individual volcanoes so in terms of what these analyses represent they are not directly comparable to our Raoul data set, however the compositional ranges are of the same order of magnitute as the Raoul samples. Values of Nb/Yb reveal that the mantle component in South Sandwich lavas ranges from as depleted as that in Raoul lavas to somewhat less depleted.

There is no indication of Zr in the subduction-related component for most South Sandwich lavas, although up to 30 % of Zr could be subduction-related in some

405 Mariana lavas. Type C arrays are formed by South Sandwich and Mariana lavas on
406 the Ba/Yb versus Nb/Yb plot, and the subduction-related contribution for Ba ranges
407 from 96 % (South Sandwich lavas) to 98 % (Mariana lavas).

408 Raoul, South Sandwich, and Mariana lavas form Type C arrays on a plot of
409 Th/Yb versus Nb/Yb (Fig. 9). For Raoul lavas, the subduction-related contribution of
410 Th ranges from a minimum of 80 % to a maximum of 90 %, and this range in Th/Yb
411 occurs at both high and low Nb/Yb. South Sandwich and Mariana lavas tend to have
412 higher subduction-related contributions for Th (up to 94 %), and both average 90 %.
413 On Ba/Yb versus Nb/Yb and Th/Yb versus Nb/Yb plots Raoul lavas form arrays that
414 indicate subduction-related contributions for Ba and Th of 96-98% and 80-90 %
415 respectively added to the depleted mantle before near-fractional melting of the mix. If
416 near-fractional melting generated the array on these plots, and the consistent
417 development of Type C arrays rather than Type B arrays on X/Yb versus Nb/Yb plots
418 provides strong evidence that this was so, then some additional component
419 replenished Ba in the melting column as it ascended. This component is inferred to be
420 the aqueous LILE-bearing fluid.

421 The arrays formed on a plot of Sr/Yb versus Nb/Yb (Fig. 9) are more
422 scattered, reflecting strong partitioning of Sr into plagioclase. For Raoul, three of four
423 representative aphyric lavas with 52-56 wt.% SiO_2 plot in the middle of the Sr/Yb
424 versus Nb/Yb array, and 70-80 % of their Sr is subduction-related. The other aphyric
425 lava has 57.8 wt.% Si0 and the lowest Sr/Yb value, probably as a result of extensive
426 plagioclase fractionation. Conversely, two basaltic slightly porphyritic lavas with 20-
427 30 % modal plagioclase and 15 % modal augite have the highest Sr/Yb values,
428 demonstrating the effect of plagioclase accumulation. The obliquity of the South
429 Sandwich array relative to the MORB array on Fig.9 suggests a strong plagioclase

fractionation effect, and these arrays are not oblique on the fractionation-corrected plot presented by Pearce et al. (1995). In contrast, most Mariana analyses do not appear strongly affected.

In summary, Raoul, South Sandwich, and Mariana lavas form Type C arrays on plots of X/Yb versus Nb/Yb, where X is Nd, La, K Pb, Rb, or Cs and a review of the subduction-related contribution for Zr, Nd, La, Sr, Th, K, Pb, Rb, Ba, and Cs is given in Table 3. A surprising feature is the consistent magnitude of the subduction-related contribution for each element in each of these arcs. Furthermore, few elements differentiate between Raoul, South Sandwich, and Mariana lavas; the largest difference occurs for Ba. This difference is sufficient to separate their arrays on the Ba/Yb versus Nb/Yb plot (Fig. 9). A more subtle difference is apparent for Th, and for this element the subduction-related contribution in Raoul lavas is slightly less than that for South Sandwich and Mariana lavas (Fig. 9).

The compositional arrays displayed by Raoul lavas in Fig.8 are interpreted as the result of addition of a subduction-related component which is of essentially constant composition and magnitude to a depleted mantle which is also of essentially constant composition (e.g. Abe et al., 1998), followed by near- fractional melting of the mix. Lavas from the South Sandwich and Mariana arcs form comparable arrays, and their subduction-related component is almost indistinguishable from that in Raoul lavas. However, the mantle beneath some South Sandwich volcanoes is less depleted, and that beneath the Mariana arc is consistently less depleted.

4. Discussion of the fractional melting model

Further insights into subduction-related magma genesis can be gained from plots of X/Z versus Nb/Yb, where X and Z are incompatible elements. If the contributions of both slab and mantle are essentially constant then early melts generated by near-fractional melting will have relatively high X/Z and high Nb/Yb for $D_x < D_z$. Later melts from the depleted melting column will have relatively low X/Z and low Nb/Yb. Analyzed lavas will then form an array of positive slope on a plot of X/Z versus Nb/Yb (i.e., increasing X/Z with increasing Nb/Yb), so long as melt pooling and mingling does not obliterate the signature of individual melt batches. In contrast, a scattergram with random trend will result if either component is of variable composition or if they are mixed in varying proportions. The array slope will be negative if $D_X > D_Z$ and the order of increasing D for the elements of interest during melting of a spinel lherzolite is taken to be Cs ~Rb ~ Ba <Th < Nb ~ K < La < Pb <Sr < Nd < Zr << Yb (Sun and McDonough, 1989).

Raoul lavas form an array with a slight negative slope on a plot of Ba/Rb versus Nb/Yb (Fig. 10) as expected, because D_{Ba} is slightly greater than D_{Rb} (Sun and McDonough, 1989). Arrays for South Sandwich and Mariana lavas are sub-parallel to that for Raoul. The Mariana array is displaced to higher Nb/Yb, whereas the South Sandwich array is displaced to lower Ba/Rb. A comparable result is obtained from a plot of Ba/Pb versus Nb/Yb (Fig. 10). The main difference between these plots is that array slopes for Ba/Pb versus Nb/Yb are positive because $D_{Ba} < D_{Pb}$ (Sun and McDonough, 1989). Values of Ba/Pb for the Raoul, South Sandwich, and Mariana arrays are more scattered than for Ba/Rb, and Ba/Pb is slightly higher for Raoul and the Mariana arrays relative to the South Sandwich array. Nevertheless, both the Ba/Rb versus Nb/Yb and Ba/Pb versus Nb/Yb plots are consistent with near-

479 fractional melting of an initially homogeneous source composition. Predicted array
480 patterns are also obtained for plots of Ba/Cs, Ba/K Ba/La, and Ba/Sr versus Nb/Yb
481 (not shown).

482 Very different behavior is apparent on a plot of Ba/Th versus Nb/Yb (Fig. 10)
483 where Raoul lavas form a well-defined array with negative slope South Sandwich and
484 Mariana lavas also form arrays with negative slope. The South Sandwich array is
485 offset to lower Ba/Th, and the Mariana array is offset to higher Ba/Th. However, D_{Ba}
486 $< D_{Th}$ (Sun and McDonough, 1989) therefore, the array slope should be positive. The
487 LILE are strongly partitioned into the aqueous fluids released during dehydration of
488 amphibole or serpentinite in the subducting slab and in general terms these elements
489 are partitioned into the fluid phase in proportion to their ionic radius. (Tatsumi et al.,
490 1986; Brenan et al., 1995; Keppler, 1996). Thus, both Th and U are expected to be
491 less mobile in the fluid phase than Ba and other LILE. Both theoretical and
492 experimental studies suggest that the solubility of Th in slab-derived aqueous fluids
493 will be less than, or at most equal to (if garnet is a residual phase in the slab), that of
494 U (Bailey and Ragnarsdottir, 1994; Brenan et al., 1995; Keppler, 1996). Isotopic
495 disequilibrium in the U-Th decay series requires at least two distinct subduction-
496 related components in intra-oceanic arc lavas one with high Ba/Nb associated with a
497 large $^{238}U/^{230}Th$ excess, and one with high Th/Nb and no ^{238}U excess (Elliott et al.,
498 1997). Regional studies of volcanic arcs also reveal a correlation of high Ba/Th with
499 low $^{87}Sr/^{86}Sr$ and low Ba/Th with high $^{87}Sr/^{86}Sr$ (Hawkesworth et al., 1997). These
500 observations lead to the conclusion that the LILE and Th are transferred from the
501 subducting slab by different mechanisms, and that their source reservoirs are distinct.
502 The LILE are thought to be rapidly transported by an aqueous fluid, whereas Th

503 resides in subducting sediment and may migrate in a siliceous melt (Elliott et al., 1997
504 Hawkesworth et al., 1997).

505 Other explanations for the Ba/Th trend are possible. For example, the
506 geochemical signature of the subduction-related component should be clearest in
507 lavas with a strongly depleted mantle component (e.g., Hawkesworth and Ellam,
508 1989). If decreasing Nb/Yb is taken as evidence of mantle depletion, then lavas with
509 low Nb/Yb might be assumed to better represent element ratios in the subduction-
510 related component. The plot of Ba/Th versus Nb/Yb could then lead to the conclusion
511 that the subduction-related component in Raoul lavas has Ba/Th> 700. However, this
512 line of reasoning cannot be valid because it implies the subduction-related component
513 is added to a variably depleted mantle component. That would generate Type B arrays
514 for Raoul lavas on X/Yb versus Nb/Yb plots, not the Type C arrays observed. Thus,
515 the Type C arrays for Raoul lavas require that any interpretation of X/Z versus Nb/Yb
516 plots reflect near-fractional melting about a mantle component of constant
517 composition.

518 This geochemical evidence leads to the conclusion that the subduction-related
519 component and the mantle- derived component are mixed in constant proportions, and
520 this mixing process presumably initiates the melting column. Increases in Ba/Th
521 during melting are attributed to continual minor inputs of a LILE-bearing fluid into
522 the melting column. The model can be tested. One prediction is that Ba/Z will
523 increase with decreasing Nb/Yb so long as Z is a conservative element, or any
524 element not present in the LILE-bearing fluid. An appropriate plot is Ba/Nb versus
525 Nb/Yb. No continual addition of LILE will yield a positive slope for the Raoul array
526 on this plot, as $D_{Ba} < D_{Nb}$ (Sun and McDonough, 1989). The negative slope on Ba/Nb

527 versus Nb/Yb (Fig. 10). indicate the continual input of a LILE-bearing component to
528 the melting column.

529 Predicted array slopes on plots of Ba/Z versus Nb/Yb depend upon D values.
530 Partition coefficients for D_{Ba} cited by Ewart et al. (1998), are $D_{Ba} > D_{Th}$ and $D_{Ba} >$
531 D_{Nb} although these relatively high values are at variance with other data compilations
532 (e.g., Sun and McDonough, 1989; McCulloch and Gamble, 1991; Stolper and
533 Newman, 1994). Published databases concur that $D_{Rb} < D_{Th}$ and $D_{Cs} < D_{Th}$ during
534 mantle melting (Sun and McDonough, 1989; McCulloch and Gamble, 1991; Stolper
535 and Newman, 1994; Ayres et al., 1997; Ewart et al., 1998; Ayres, 1998). Raoul lavas
536 form arrays of negative slope on plots of Rb/Th versus Nb/Yb and Cs/Th versus
537 Nb/Yb, although with appreciable scatter. Therefore, replenishment of both Rb and Cs
538 relative to Th is also required in the ascending melting column, supporting the
539 evidence provided by changes in Ba/Th.

540 A further test is provided by changes in radiogenic isotope ratios with Nb/Yb.
541 None of the analyzed radiogenic isotopes ($^{87}/_{86}Sr$, $^{143}/_{144}Nd$, $^{206}/_{204}Pb$, $^{207}/_{204}Pb$,
542 $^{208}/_{204}Pb$) show any correlation with SiO_2 or other major or trace element
543 concentrations in Raoul lavas. However, Raoul lavas form an array with negative
544 slope on a plot of $^{87}/_{86}Sr$ versus Nb/Yb (Fig11). The higher $^{87}/_{86}Sr$ values of lavas
545 with low Nb/Yb, which are those melts generated at a relatively late stage from the
546 melting column, is best explained by the continual addition of a small amount of
547 L1LE-bearing fluid with high $^{87}/_{86}Sr$ to the melting column. The South Sandwich
548 array also has a negative slope for $^{87}/_{86}Sr$ versus Nb/Yb. Other analyzed radiogenic
549 isotopes do not show significant correlations with Nb/Yb, although the slope of the
550 Raoul array for $^{206}/_{204}Pb$ versus Nb/Yb is slightly positive (Fig. 11).

In conclusion, the geochemical arrays formed by Raoul lavas on plots of X/Z versus Nb/Yb are best interpreted in terms of a near-fractional melting model. These plots require one subduction-related component for the LILE (Sr, K, Pb, Rb, Ba, Cs) and another for Th. Furthermore, they indicate continual minor addition of LILE-bearing fluid to the melting column as it ascends, but no replenishment of Th (or conservative elements). Higher $^{87}/_{86}Sr$ in late stage melts from the column also testifies to the continual addition of a LILE-bearing fluid. Similar trends are shown by South Sandwich and Mariana lavas.

5. Discussion

5.1 Origin of mantle depletion

Subduction-related magmas from intra-oceanic arcs with active backarc basins, such as the Tonga-Kermadec arc, are characterized by a depleted mantle component (Ewart and Hawkesworth, 1987; McCulloch and Gamble, 1991; Pearce and Parkinson, 1993; Woodhead et al., 1993). Some conservative elements in Raoul lavas are mildly depleted relative to FMM (e.g., Nb, Zr, Ti), but this depletion is restricted to those elements with $D_C < D_Y$ during mantle melting. Conservative elements that are highly sensitive to mantle melting and depletion events have concentrations consistent with the generation of Raoul primary magmas by 15-35 % melting of FMM from which a melt fraction of up to 4 % has previously been extracted. However, Raoul lavas form Type C arrays on plots of X/Yb versus Nb/Yb. Such arrays indicate near-fractional melting of a homogeneous source, and cannot ordinarily be produced by melting of variably depleted mantle mixed with a subduction-related component.

These observations can be reconciled by re-interpreting mantle melting and depletion in terms of a near-fractional melting process from which early formed melts have high Nb and Yb in contrast with later melts from the melting column which will have relatively low Nb and Yb The dimensions of the Raoul array on Fig. 6 are thus an artefact of fractional melting about a mid point composition. The true mantle composition is FMM from which a ~2 % melt fraction has previously been extracted. Similarly, the range in Nb/Yb of 0.13-0.33 is interpreted as an artefact of fractional melting about a homogeneous source with average Nb/Yb of 0.22 (e.g., Type C behaviour on fig 8), this compares with a MORB Nb/Yb of 0.76 (Pearce and Parkinson, 1993).

The origin of mantle depletion beneath intra-oceanic arcs has been much discussed (e.g., Ewart and Hawkesworth, 1987; McCulloch and Gamble, 1991; Pearce and Parkinson, 1993; Woodhead et al., 1993; Elliott et al., 1997). Potentially, mantle depletion may occur by:

1) progressive melt extraction from sub-arc mantle, coupled with minimal advection of fresh material into the sub-arc zone.
2) melt extraction from a melting column beneath the spreading centre of a backarc basin, followed by advection of depleted mantle into the sub-arc zone.
3) recycling of depleted mantle residue from the sub-arc melting column through the mantle wedge and back into the melting column.
4) continual loss of early formed melts from the base of the sub-arc melting column.

There is a general consensus that (2) is the dominant process, and this is strongly supported by the occurrence of undepleted or enriched mantle components in subduction-related magmas from intra-oceanic arcs that lack active backarc basins,

599 such as the West Aleutian and Vanuatu arcs. Some consider (4) may also be
600 significant (Pearce and Peate, 1995).

601 Key conclusions reached for the mantle component in Raoul lavas are that the
602 degree of depletion is minor and of constant magnitude with time. These are
603 inconsistent with (1), in which mantle depletion would increase with time, and with
604 (3), in which variable and random mantle depletion with time is more likely. Instead,
605 the rate of mantle advection must be sufficient that a new unit of homogeneous mildly
606 depleted mantle replenishes the base of the melting column for each unit that begins
607 to melt and ascend.

608 The generation of homogeneous mildly depleted mantle beneath a backarc
609 spreading centre is not problematic. Trace element concentrations in the
610 clinopyroxene of abyssal peridotites (mantle residue) indicate that small melt fractions
611 (0.1-1.0 %) readily segregate from mantle melting columns (Johnson et al., 1990).
612 Thus, melt extraction beneath a back arc spreading centre produces a homogeneous
613 depleted residue. The extent of depletion will depend upon the average height to
614 which the melting column ascends (extent of decompression) and its temperature
615 (Klein and Langmuir, 1987; McKenzie and Bickle, 1988). If the rate of mantle
616 advection is driven by the down-drag of mantle adjacent to the subducting slab (e.g.,
617 Davies and Stevenson, 1992), and spreading centers beneath active backarc basins
618 represent passive mantle upwelling, then it is reasonable to expect a relationship
619 between the rate of backarc extension and mantle depletion because faster extension
620 at a fixed subduction rate will allow mantle in the backarc basin melting column to
621 rise higher and undergo more melting before it is advected out of that column and
622 towards the sub-arc melting column.

623 Subduction rates beneath Raoul and the South Sandwich and central Mariana arcs
624 are essentially identical, whereas backarc extension rates vary (Table 4). Taking
625 Nb/Yb as an indicator of mantle depletion, Raoul has the most depleted mantle
626 composition and the lowest backarc extension rate. Comparable subduction and
627 backarc extension rates for Raoul and the central Mariana arc should result in
628 similarly depleted mantle components, but Raoul lavas [average Nb/Yb = 0.22] are
629 markedly more depleted than those of the Mariana arc [average Nb/Yb = 0.49]. Some
630 of this difference arises from the comparison of data from a single volcano (Raoul)
631 with databases consisting of few analyses from many volcanoes (South Sandwich and
632 Mariana).

633 In summary, the sub-arc mantle beneath Raoul is required to be homogeneous and
634 to advect rapidly into the sub-arc melting column in order to avoid the development of
635 a long term depletion trend, and to be mildly depleted with respect to FMM (Nb/Yb =
636 0.22). A comparison with lavas from the intra-oceanic South Sandwich and Mariana
637 arcs reveals no obvious link between the degree of mantle depletion and the
638 subduction rate, backarc extension rate, or backarc basin width. We suggest that
639 further sampling of the Tonga-Kermadec arc and modelling of geochemical analyses
640 in terms of near-fractional melting will provide the means to unlock this puzzle. In
641 particular, the middle section of the arcs (from L'Esperance Rock to 'Ata Island)
642 provides an opportunity to examine conservative element co-variations as from south
643 to north the backarc extension half-rate increases from 1.9 to 6.5 cm per year and the
644 subduction rate increases from 7.2 to 13.5 cm per year, the latter predominantly in
645 response to the higher rate of backarc extension. The mantle composition has Pacific
646 MORB-source affinities throughout this part of the arc (Smith and Price, 2006 and
647 references therein).

5.2 Buffering of the subduction-related component

The distinctive high LILE/HFSE ratios of subduction-related magmas compared with MORB are generally attributed to the transfer of a hydrous LILE-bearing component from the subducting slab to the overlying mantle (e.g., Tatsumi et al., 1986; McCulloch and Gamble, 1991; Pearce and Peate, 1995). The relative proportion of each element contributed by the subduction-related component can be assessed from plots of X/Yb versus Nb/Yb, where X is an incompatible element. Negligible Zr, 30 % of the Nd, 55 % of the La, 75 % of the Sr, 85 % of the Th, and >90 % of the K, Pb, Rb, Ba, and Cs in Raoul lavas is subduction-related. Furthermore, the arrays generated on these plots are consistently parallel to the MORB array and offset from it by a constant proportion to higher X/Yb. Arrays of this type require tight coupling between X/Yb and Nb/Yb which, except under extraordinary circumstances, can only be provided by the relative distribution during mantle melting. Therefore, they indicate a constant subduction-related component added to a constant mantle composition, followed by near-fractional melting of the mix (Pearce et al., 1995).

Sources of the subduction-related component are the altered oceanic crust of the subducting slab and its overlying sediment veneer. Fluids or melts generated in either of these are likely to have distinct compositions that vary with depth of origin within each source, and with the PT conditions of the slab. Thus, some mechanism must exist to transform part (or all) of the slab-derived flux into a homogeneous subduction-related component as it migrates from the slab-mantle interface to the base of the melting column. Fluid (or melt) passing through the mantle will react with it to attain chemical equilibrium. Two possible types of reactions are considered.

In the first, the interaction is analogous to the operation of a chromatographic column (Navon and Stolper, 1987; Hawkesworth et al., 1994). Elements in the fluid

673 (or melt) migrate through the mantle chromatograph at rates inversely proportional to
674 their bulk mantle-fluid partition coefficients. Because the mantle is advecting, there is
675 a critical value for this parameter such that elements with distribution coefficients less
676 than the critical value do not exit the chromatograph before advection carries them
677 beyond the sub-arc melting column. These elements remain within the mantle,
678 whereas the others exit as the subduction-related component. However, the rate of
679 element migration through the chromatograph is not concentration dependent and
680 therefore, this mechanism is incapable of buffering the composition of the subduction-
681 related component in real-time. Slab-derived elements either exit the chromatograph
682 at the base of the melting column if their distribution coefficient is less than the
683 critical value or else they do not. Temporal changes in the slab-derived flux as it
684 enters the chromatograph are preserved in element concentration profiles at the exit
685 point, although element-element ratios are decoupled.

686 A second type of interaction features fluid (or melt) reacting with mantle
687 peridotite to form amphibole (Tatsumi et al., 1986; Davies and Bickle, 1991; Davies
688 and Stevenson, 1992).). Mantle advection carries this metasomatised peridotite
689 formed adjacent to the subducting slab to progressively deeper levels until amphibole
690 decomposes at 3.0 GPa. An aqueous fluid (or melt if T> 1000 °C), is released and
691 ascends vertically until it reaches amphibole-undersaturated mantle at lower pressure,
692 whereupon fluid (or melt) reacts with peridotite to form new amphibole. The process
693 repeats until the PT conditions of the amphibole- saturated peridotite solidus are
694 reached at the base of the sub-arc melting column (3.0 GPa, 1150°C). The
695 composition of the fluid (or melt) is controlled by the number of cycles in which
696 amphibole decomposes to pyroxene. Therefore, slab-derived material transported by
697 this process should reflect $D_{pyroxene}$ when it the reaches the melting column.

698 Recent experiments indicate that clinpoyroxene distribution coefficients in
699 alkali chloride-rich fluids increases in the sequence La < Sr < Th <Pb < K < Ba < Rb,
700 and $D_{La} \sim 1$ at 0.3 GPa and 1040 °C (Keppler, 1996; Kessel et al., 2005). This
701 sequence closely resembles that of the increasing subduction-related contribution in
702 Raoul lavas of La < Sr < Th <K < Pb < Rb <Ba. Increasing pressure from 0.3 to 2.0
703 GPa changes D by less than an order of magnitude, but further experiments are
704 needed to assess the dependence of the element sequence on pressure, fO_2, and
705 chloride concentration (Keppler, 1996). Combined amphibole-fluid (melt) transport
706 from the mantle-slab interface to the melting column appears to be the most likely
707 mechanism by which the slab-derived flux is converted to the homogeneous
708 subduction-related component mixed with the mantle at the base of the melting
709 column beneath Raoul.

710 The remarkable similarity between the subduction-related contribution for
711 Raoul and that for the South Sandwich and Mariana arcs is consistent with buffering
712 of the slab-derived flux by pyroxene distribution coefficients beneath these arcs
713 However, subtle differences do exist. Chief amongst these is the Ba-rich nature of
714 Raoul and Mariana lavas relative to those of the South Sandwich arc (Fig.9). This is
715 of sufficient magnitude that their arrays are just separated on plots of Ba/Yb versus
716 Nb/Yb and Ba/Z versus Nb/Yb, where Z is any incompatible element. Raoul and
717 Mariana lavas are also slightly Th-poor relative to South Sandwich lavas and Mariana
718 lavas are richer in Zr and the REE than either Raoul or South Sandwich lavas (Fig 9).

719 There are differences in the character of the subducting slab beneath Raoul
720 and the South Sandwich and Mariana arcs. Altered oceanic crust subducting beneath
721 Raoul and the Mariana arc is of comparable age, whereas that subducting beneath the
722 South Sandwich arc is appreciably younger (Table 5). Nonetheless, hydrothermal

723 alteration of oceanic crust is most rapid at mid-ocean ridges, is completed in <70 Ma,
724 and is probably independent of the spreading rate (e.g., Stein and Stein, 1994; German
725 et al., 1995). Therefore, inter-arc changes in the fluid or melt flux emanating from
726 subducting oceanic crust are not expected. Major inter-arc differences occur in the
727 thickness and composition of subducting sediments (Table 5). Two estimates of the
728 sediment flux beneath Raoul have been calculated. One utilises the average
729 composition of sediment from DSDP 204 (100 km east of Tonga), and the other that
730 from DSDP 595/596 (950 km east of Tonga). The calculated fluxes differ markedly
731 (e.g., Ba_{flux}/Th_{flux} = 52-173, Ba_{flux}/Rb_{flux} = 7-43), and typically bracket those of the
732 South Sandwich and Mariana arcs.

733 In summary, the main subduction-related contribution in Raoul lavas is of
734 constant composition and magnitude. This is consistent with material derived from the
735 subducting oceanic crust and its sediment veneer being transported from the slab-
736 mantle interface to the base of the sub-arc melting column by alternating episodes of
737 amphibole formation and amphibole decomposition to pyroxene with fluid release,
738 leading to further amphibole formation. The composition of the subduction-related
739 component reaching the melting column is thus buffered by pyroxene distribution
740 coefficients. Subtle differences in the subduction-related contribution between Raoul
741 and the South Sandwich and Mariana arcs resemble changes in the bulk composition
742 of subducting sediment, but sediment compositions are poorly constrained.

743 *5.3 Role of amphibole-saturated peridotite*

744 The co-variation of X/Yb with Nb/Yb, where X is an incompatible element
745 leads to the conclusion that magma genesis beneath Raoul involves near- fractional
746 melting of mildly depleted mantle mixed with a subduction-related component.
747 Neither component varies significantly in composition through the exposed sequence

748 on Raoul Volcano. In addition, both components must be mixed in set proportions for
749 Type C arrays to develop in preference to Type A arrays (Fig. 8). Thus, upwelling of
750 the melting column is apparently initiated by the addition of a fixed amount of the
751 subduction-related component to the mantle.

752 This constraint is difficult to explain if slab-derived fluid or melt migrates
753 freely from the slab-mantle interface to the base of the melting column, or by
754 chromatographic exchange reactions. Temporal changes in the flux of H_2O and other
755 elements, reflecting heterogeneity in the subducting slab, would be a reasonable
756 expectation in both cases. However, a very different outcome arises if the slab-derived
757 flux is transported to the base of the melting column by amphibole.

758 Mantle peridotite in the wedge reacts with fluid (or melt) from the subducting
759 slab until amphibole-saturation is attained (Tatsumi et al., 1986; Davies and Bickle,
760 1991; Davies and Stevenson, 1992). Excess fluid (or melt) will ascend until it reaches
761 amphibole-undersaturated mantle. Amphibole is repeatedly decomposed when down-
762 dragged to 3.0 GPa, releasing a fluid or melt, and subsequently re-formed at lower
763 pressures.. Eventually, amphibole decomposition occurs at the PT conditions that
764 mark the amphibole-saturated peridotite solidus and define the base of the sub-arc
765 melting column (3.0 GPa, 1150 °C). If sufficient fluid is transferred from the slab,
766 then all mantle peridotite passing through the base of the melting column will be
767 amphibole-saturated and contain a fixed modal proportion of amphibole. This is
768 equivalent to a fixed unit of the subduction-related component mixed with a fixed unit
769 of the mantle. Furthermore, this amphibole-saturated peridotite will have a fixed H_2O
770 content, and the composition of the subduction-related component will be buffered by
771 pyroxene distribution coefficients

772 Our observations and calculations indicate that in this model a 2-8 % melt
773 fraction is generated at the amphibole-saturated solidus, with 1.6-6.0 wt.% H_2O in the
774 melt (Davies and Bickle, 1991). The H_2O content in this initial melt fraction is
775 significantly greater than that estimated for primitive subduction-related magmas of 2-
776 4 wt.% H_2O (Davies and Stevenson, 1992; Sisson and Grove, 1993). Decompression
777 melting of MORB source mantle results in up to 18 % melting for long melting
778 columns (Kinzler and Grove, 1992). By analogy, this will augment the initial melt
779 formed at the base of the sub-arc melting column and dilute its H_2O content. A
780 magma may also exsolve H_2O as it rises (e.g., Sisson and Grove, 1993).

781 We suggest that excess H_2O in the initial melt may play another role. Plots of
782 X/Z versus Nb/Yb, where X and Z are incompatible elements, indicate continued
783 replenishment of the melting column by a LILE-rich component. This component is
784 of small magnitude relative to the total subduction-related component. Potentially,
785 aqueous fluid released during amphibole decomposition at the base of the sub-arc
786 melting column exceeds H_2O saturation of the melt. An aqueous fluid with the
787 composition of the subduction-related component could then exist as a free phase, and
788 percolate to higher levels until encountering H_2O undersaturated conditions within the
789 mantle-melt mix. The rapid upwards percolation of a free aqueous phase may be
790 important in the development of U-Th isotopic disequilibrium, which require a very
791 short transit time of 30-120 ka. for U and other LILE from the subducting slab to
792 eruption (Hawkesworth et al., 1997).

793

794 **6. Conclusion**

795 The genesis of magmas in subduction zones is ultimately the result of the
796 interaction of recycled oceanic crust and the overlying mantle wedge. The product of
797 this interaction is primitive arc-type magma although because of crustal processes this
798 is typically profoundly modified in its passage toward the surface (eg Price et al.,
799 2005). In this paper we have used the variation in trace element abundances in a
800 single magmatic system to assess the relative contribution of different components to
801 magma genesis in a simple tectonic setting where evolved continental crust is absent.

802 Key findings are that:

803 1. Magmas are produced within the mantle wedge by near fractional
804 melting triggered by the release of fluids at the amphibole breakdown
805 point. For Raoul Volcano this source is depleted in incompatible
806 elements by about 2% relative to fertile MORB mantle.

807 2. A subduction-related component of constant composition and
808 magnitude has been added to this mantle source. A homogeneous
809 subduction-related component of constant composition and magnitude
810 is produced if the slab-derived fluid flux migrated into the slab-mantle
811 interface to the sub-arc melting column by repeated episodes of
812 amphibole formation and decomposition and its composition is then
813 governed by pyroxene distribution coefficients. The remarkably
814 similar composition and magnitude of the subduction-related
815 component in Raoul, South Sandwich and Mariana lavas despite
816 variations in subducting sediment flux testifies to the buffering effect
817 of this transfer mechanism.

3. A second and more mobile LILE-bearing component is continuously added to the meld column and this is also responsible for higher $^{87}/_{86}Sr$. Similar trends are shown by South Sandwich and Mariana lavas.

References

Abe, N., Ari, S., Yurimoto, H., 1998. Geochemical characteristics of the uppermost mantle beneath the Japan island arcs: implications for upper mantle evolution. Physics of the Earth and Planetary Interiors 107: 233-248.

Ayres, J. 1998. Trace element modeling of aqueous fluid-peridotite interaction in the mantle wedge of subduction zones. Contributions to Mineralogy and Petrology 132:390-404.

Ayres, J.C., Dittmer, S. K., Layne, G.D. 1997. Partitioning of elements between peridotite and H_2O at 2.0-3.0 GPa and 900-1100^oC, and application to models of subduction zone process. Earth and Planetary science Letters 150: 381-398.

Bailey, E.H. and Ragnarsdottir, K.V. 1994. Uranium and thorium solubilities in subduction zone fluids. Earth and Planetary Science Letters 124, 119-129.

Barker, P.F. 1995. Tectonic framework of the East Scotia Sea. In: Taylor, B. (editor) Backarc Basins: Tectonics and Magmatism. Plenum Press, New York, 281-314.

Ben Othman, D., White, W.M. and Patchett, J. 1989. The geochemistry of marine sediments, island arc magma genesis, and crust-mantle recycling. Earth and Planetary Science Letters 94: 1-21.

Brenan, J.M., Shaw, H.F., Phinney, D.L. and Ryerson, F.J. 1995. Mineral-aqueous fluid partitioning of trace elements at 900 °C and 2.0 GPa: constraints on the

trace element chemistry of mantle and deep crustal fluids. Geochimica et Cosmochimica Acta 59: 3331-3350.

Carmichael, I.S.E. and Ghiorso, M.S. 1990. The effect of oxygen fugacity on the redox state of natural liquids and theirI crystallising phases. Reviews in Mineralogy 24: 191-212.

Caulfield, J.T., Turner, S.P., Dosseto, A., Pearson, N.J., Beier, C. 2008. Source depletion and extent of melting in the Tongan sub-arc mantle. Earth and Planetary Science Letters 273: 279-288.

Davies, J.H. 1999. The role of hydraulic fractures and intermediate depth earthquakes in generating subduction zone magmatism. Nature 398: 142-145.

Davies, J.H. and Bickle, M.J. 1991. A physical model for the volume and composition of melt produced by hydrous fluxing above subduction zones. Philosophical Transactions of the Royal Society of London A355: 355-364.

Davies, J.H. and Stevenson, D.J. 1992. Physical model of source region of subduction zone volcanics. Journal of Geophysical Research 97: 2037-2070.

Eichelberger, J. C. Izbekov, P. E. Browne, B. L. *2006.* Bulk chemical trends at arc volcanoes are not liquid lines of descent. Lithos, 87: 135-154.

Elliott, T., Plank, T., Zindler, A., White, W. and Bourdon, B. 1997. Element transport from slab to volcanic front at the Mariana arc. Journal of Geophysical Research 102: 14991-15019.

Ewart, A. and Hawkesworth, C.J. 1987. The Pleistocene-Recent Tonga-Kermadec arc lavas: interpretation of new isotopic and rare earth data in terms of a depleted mantle source model. Journal of Petrology 28: 495-530.

Ewart, A., Collerson, K.D., Regelous, M., Wendt, J.I. and Niu, Y. 1998. Geochemical evolution within the Tonga- Kermadec-Lau arc-back-arc systems: the role of

varying mantle wedge composition in space and time. Journal of Petrology 39: 331-368.

Fryer, P. 1995. Geology of the Mariana Trough. In: Taylor, B. (editor) Backarc Basins: Tectonics and Magmatism. Plenum Press, New York, 237-279.

German, C.R., Baker, E.T. and Klinkhammer, G. 1995. Regional setting of hydrothermal activity. In: Parson, L.M., Walker, C.L. and Dixon, D.R. (eds) Hydrothermal Vents and Processes. Geological Society, Special Publication 87: 3-15.

Gill, J.B. 1981. Orogenic Andesites and Plate Tectonics. Springer-Verlag, New York, 390 pp.

Handley, H., Turner, S., Smith, I., Stewart, R., Cronin, S.J., 2008. Rapid timescales of differentiation and evidence for crustal contamination at intra-oceanic arcs: geochemical and U-Th-Ra-Sr-Nd isotopic constraints from Lopevi Volcano, Vanuatu, SW Pacific. Earth and Planetary Science Letters 273, 184-194.

Hawkesworth, C.J. and Ellam, R.M. 1989. Chemical fluxes and wedge replenishment rates along Recent destructive plate margins. Geology 17: 46-49.

Hawkesworth, C.J., Hergt, J.M., Ellam, R.M. and McDermott, F. 1991. Element fluxes associated with subduction related magmatism. Philosophical Transactions of the Royal Society of London A335: 393-405.

Hawkesworth, C.J., Gallagher, K., Hergt, J.M. and McDermott, F. 1994. Destructive plate margin magmatism:I geochemistry and melt generation. Lithos 33: 169-188.

Hawkesworth, C., Turner, S., Peate, D., McDermott, F. and van Calsteren, P. 1997. Elemental U and Th variations in island arc rocks: implications for U-series isotopes. Chemical Geology 139: 207-221.

Hergt, J.M. and Hawkesworth, C.J. 1994. Pb-, Sr-, and Nd-isotopic evolution of the Lau Basin: implications for mantle dynamics during backarc opening. In: Hawkins, J.W., Parson, L.M., Allan, J.F., et al. (editors) Proceedings of the Ocean Drilling Program, Scientific Results 135. College Station, TX: Ocean Drilling Program, 505-517.

Johnson, K.T.M., Dick, H.J.B. and Shimizu, N. 1990. Melting in the oceanic mantle: an ion microprobe study of diopsides in abyssal peridotites. Journal of Geophysical Research 95: 2661-2678.

Keppler, H. 1996. Constraints from partitioning experiments on the composition of subduction-zone fluids. Nature 380: 237-240.

Kessel, R., Schmidt, M. W., Ulmer, P., Pettke, T. 2005. Trace element signature of subduction-zone fluids, melts and supercritical liquids at 120–180 km depth. Nature 437, 724-727.

Kinzler, R.J. and Grove, T.L. 1992. Primary magmas of mid-ocean ridge basalts. 2. Applications. Journal of Geophysical Research 97: 6907-6926.

Klein, EM. and Langmuir, C.H. 1987. Global correlations of ocean ridge basalt chemistry with axial depth and crustal thickness. Journal of Geophysical Research 94: 8089-8115.

Klein, EM. and Langmuir, C.H. 1989. Local versus global variations in ocean ridge basalt composition: a reply. Journal of Geophysical Research 94: 4241-4252.

McCulloch, M.T. and Gamble, J.A. 1991. Geochemical and geodynamical constraints on subduction zone magmatism. Earth and Planetary Science Letters 102: 358-374.

McDermott, F., Defant, M.J., Hawkesworth, C.J. and Maury, R.C. 1993. Isotope and trace element evidence for three component mixing in the genesis of the North

Luzon arc lavas (Philippines). Contributions to Mineralogy and Petrology 113: 9-23.

McKenzie, D. and Bickle, M.J. 1988. The volume and composition of melt generated by extension of the lithosphere. Journal of Petrology 29: 625-679.

Navon, 0. and Stolper, E. 1987. Geochemical consequences of melt percolation: the upper mantle as a chromatographic column. Journal of Geology 95: 285-307.

Nichols, G.T., Wyllie, P.J. and Stern, CR. 1994. Subduction zone melting of pelagic sediments constrained by melting experiments. Nature 371: 785-788.

Norrish, K., Hutton, J.T. 1969. An accurate X-ray spectrographic method for the analysis of a wide range of geological samples. Geochimica et Cosmochimica Acta 33: 431-453.

O'Hara, M.J. 1985. Importance of the "shape" of the melting regime during partial melting of the mantle. Nature 314: 58-62.

Parson, L.M. and Wright, I.C. 1996. The Lau-Havre-Taupo back-arc basin: a southward-propagating, multi-stage evolution from rifting to spreading. Tectonophysics 263: 1-22.

Pearce, J.A. 1983. Role of the sub-continental lithosphere in magma genesis at active continental margins. In: Hawkesworth, C.J. and Norry, M.J. (eds) Continental Basalts and Mantle Xenoliths. Shiva Publishing, Nantwich, 230-249.

Pearce, J.A. and Parkinson, I.J. 1993. Trace element models for mantle melting: application to volcanic arc petrogenesis. In: Prichard, H.M., Alabaster, T., Harris, N.B.W. and Neary, C.R. (editors) Magmatic Processes and Plate Tectonics. Geological Society, Special Publication 76: 373-403.

941 Pearce, J.A. and Peate, D.W. 1995. Tectonic implications of the composition of
942 volcanic arc magmas. Annual Review of Earth and Planetary Science 23: 251-
943 285.
944 Pearce, J.A., Baker, P.E., Harvey, P.K. and Luff, I.W. 1995. Geochemical evidence
945 for subduction fluxes, mantle melting and fractional crystallisation beneath the
946 South Sandwich island arc. Journal of Petrology 36: 1073-1109.
947 Pearce, J.A., Kempton, P.D., Gill, J.B. 2007. Hf-Nd evidence for the origin and
948 distribution of mantle domains in the SW Pacific. Earth and Planetary science
949 Letters 260: 98-114.
950 Peate, D.W., Pearce, J.A., Hawkesworth, C.J., Colley, H., Edwards, C.M.H. and
951 Hirose, K. 1997. Geochemical variations in Vanuatu arc lavas: the role of
952 subducted material and a variable mantle wedge composition. Journal of
953 Petrology 38: 1331-1358.
954 Plank, T. and Langmuir, C.H. 1993. Tracing trace elements from sediment input to
955 volcanic output at subduction zones. Nature 362: 739-743.
956 Price, R. C., Gamble, J. A., Smith, I.E.M., Eggins, S.,. Wright, I.C. 2005. An
957 integrated model for the temporal evolution of andesites and rhyolites and
958 crustal development in New Zealand's North Island. Journal of Volcanology
959 and Geothermal Research 140: 1-24.
960 Shevais, J.W. 1982. Ti-V plots and the petrogenesis of modern and ophiolitic lavas.
961 Earth and Planetary Science Letters 59: 101-118.
962 Sisson, T.W. and Grove, T.L. 1993. Temperatures and H contents of low-MgO high-
963 alumina basalts. Contributions to Mineralogy and Petrology 113: 167-184.
964 Smith, I.E.M., Price, R.C., 2006. The Tonga-Kermadec arc and Havre Lau back arc
965 system: Their role in the development of tectonic and magmatic models for the

966 western Pacific Journal of Volcanology and Geothermal Research 156: 315-
967 331.
968 Smith, I. E. M., Worthington, T. J. Price , R. C., Stewart, R. B., Maas, R. 2006.
969 Petrogenesis of Dacite in an oceanic subduction environment: Raoul Island,
970 Kermadec Arc Journal of Volcanology and Geothermal Research 156: 252-
971 265.
972 Stein, C.A. and Stein, S. 1994. Constraints on hydrothermal heat flux ough the
973 oceanic lithosphere from global heat flow. Journal of Geophysical Research
974 99, 3081-3095.
975 Stolper, E. and Newman, S. 1994. The role of water in the petrogenesis of Mariana
976 trough magmas. Earth and Planetary Science Letters 121: 293-325.
977 Sun, S-s. and McDonough, W.F. 1989. Chemical and isotopic systematics of oceanic
978 basalts: implications for mantle composition and processes. In: Saunders, AD,
979 and Norry, M.J. (editors) Magmatism in the Ocean Basins. Geological
980 Society, Special Publication 42: 313-345.
981 Tatsumi, Y., Hamilton, D.L. and Nesbitt, R.W. 1986. Chemical characteristics of
982 fluid phase released from a subducted lithosphere and origin of arc magmas:
983 evidence from high-pressure experiments and natural rocks. Journal of
984 Volcanology and Geothermal Research 29: 293-309.
985 Turner, S.P. and Hawkesworth, C.J. 1995. The nature of the sub-continental mantle:
986 constraints from the major-element composition of continental flood basalts.
987 Chemical Geology 120: 295-314.
988 Turner, S.P. and Hawkesworth, C.J. 1997. Constraints on flux rates and mantle
989 dynamics beneath island arcs from Tonga-Kermadec lava geochemistry.
990 Nature 389: 568-573.

Turner, S.P., Hawkesworth, C.J., van Calsteren, P., Heath, E., Macdonald, R. and Black, 5. 1996. U-series isotopes and destructive plate margin magma genesis in the Lesser Antilles. Earth and Planetary Science Letters 142: 191-207.

Turner, S.P., Hawkesworth, C.J., Rogers, N., Bartlett, J., Worthington, T.J., Hergt, J., Pearce, J.A. and Smith, I.E.M. 1997. ^{238}U disequilibria, magma petrogenesis, and flux rates beneath the depleted Tonga-Kermadec island arc. Geochimica et Cosmochimica Acta 61: 4855-4884.

Woodhead, J.D., Eggins, S.M. and Gamble, J.A. 1993. High field strength and transition element systematics in island arc and back-arc basin basalts: evidence for multi-phase melt extraction and a depleted mantle wedge. Earth and Planetary Science Letters 114: 491-504.

Appendix 1. Analytical methods

Samples were washed and dried to remove possible sea-spray contamination and crushed in a tungsten carbide ring grinder. H_2O^- and loss on ignition (LOI) were determined by weight loss after heating to 115^{o}C and 950^{o}C respectively. Major elements were analyzed using fused glass discs (La-doped lithium tetra borate/ lithium metaborate flux) by X-ray Fluorescence at University of Auckland (Phillips PW1410 wavelength-dispersive spectrometer) using standard matrix correction procedures. For a typical Raoul lava the precision (1σ) of the major elements is better than 0.5% for SiO_2, 0.5-1.0 % for TiO_2, Al_2O_3, Fe_2O_3 and CaO, 1-3% for MgO, Na_2O and K_2O and 308% for MnO and P_2O_5.

Minor trace elements were analyzed in solution at Monash University using the VG Plasmaquad $PQ2^+$ spectrometer. Sample preparation involved digesting in an HF-

HNO_3 mix, evaporating to dryness, refluxing twice in concentrated HNO_3 before taking up in 50 ml of 2% HNO_3 for a final dilution factor of approximately 2000. ^{115}In was used as an internal standard. The precision (1σ) is 4-7% for REE, Hf and Pb, 7-12% for Ge, Rb, Nb, Cs, Ta, Th and U, and 1-4% for the remainder. Detection limits are less that ~10ppb. The precision of each analysis was provided by VIEPS (Victoria Institute of Earth and Planetary Science) in-run standard deviation/average analysis.

Isotopic analyses were analyzed by thermal ionization mass spectrometry. Samples were leached in 4 ml of 5.25N HNO_3 and rinsed with deionised water to guarantee no residual contamination from sea spray. The leached sample was digested in 2 ml of 40% HF and evaporates to dryness; this step was repeated. A further 1 ml of 40% HF combined with 2 ml concentrated HNO_3 was added and evaporated at 110^{o}C until dissolution was complete and the solution was then divided equally into a Sr+Nd and a Pb split before evaporation to dryness. The Sr+Nd split was redissolved in 2 ml of 1N HCl and cation chromatography used to generatet Sr and Nd concentrates. The Pb split was redissolved in 1N HCl and Pb extracted using conventional HBr-HCl column chemistry. All Sr, Nd, and Pb isotope ratios were analyzed using the Finnegan-MAT 262 multicollector mass spectrometer at La Trobe University. Three Sr-Nd and four Pb procedural blanks were analysed, these reported Sr<2 ng, Nd<50pg and Pb<0.8 ng. No blank corrections have been applied as the blank levels were negligible relative to the sample sizes used. During the course of this analytical work NBS987 reported $^{86}/_{87}Sr$ ratios = 0.71024 $\pm$ 0.00003 (n=7) compared to a long term laboratory average of 0.71024 $\pm$ 0.00004 and an accepted ratio of 0.71024. Repeated analysis of La Jolla reported $^{143}/_{144}Nd$ = 0.511855 $\pm$ 0.000006 (n=3) compared to a long term laboratory average of 0.511857 $\pm$ 0.000002 and an accepted ratio of

0.511850. For Pb the average errors in analyses of NBS981 were 0.10% for $^{206}/_{204}$Pb, 0.13% for $^{207}/_{205}$Pb amd 0.18% for $^{208}/_{204}$Pb (n=78 for the laboratory. All errors quoted are 2σ of the mean.

Figure captions

1. Tectonic setting of Raoul Island vs trench and ridge. The active and remnant arcs of the region and the Louisville seamount chain are defined topographically by the 2000 m bathymetric contour and the Kermadec and Tonga trenches are defined by the 7000 m bathymetric contour. TVZ signifies the Taupo Volcanic Zone of central North Island New Zealand.

2. Plot of Mg# (mol.% MgO/(MgO+FeO)) against SiO_2 for all Raoul Volcano lavas. Samples with high Mg# and low SiO_2 have high phenocryst contents (40-50 vol.%) and their apparently primitive compositions reflect mafic mineral accumulation.

3. Fertile MORB Mantle (FMM) source normalized plot for conservative elements in aphyric (darker shading) and slightly porphyritic (lighter shading) Raoul lavas. Elements are plotted in order of increasing D_C (distribution coefficient for conservative elements). The FMM composition, the MORB composition and the element order are taken from Pearce and Parkinson (1993). Raoul lavas are depleted in those elements more incompatible than Y relative to MORB but not for other conservative elements.

4. Al_8 / Ti_8 versus Ca_8 / Ti_8 for Raoul lavas. Aphyric lavas (solid circles) plot alongside MORB and do not require re-melting of a depleted mantle source (MORB value at 7.5 wt.% MgO calculated from Pearce and Parkinson, 1993). Progressively more porphyritic lavas (open squares) plot in an array extending

to higher values of both ratios.Vectors depict plagioclase, clinopyroxene, and olivine accumulation. Fields for experimental fertile and depleted mantle melts regressed to MgO = 8 wt.% (Hawaiian pyrolite and Tinaquillo lherzolite, respectively), and the Tonga-Kermadec arrays (lighter stipple uncorrected for crystal accumulation), are after Turner et al., (1997) and references therein.

5. Na_8 versus Fe_8 for Raoul lavas. Aphyric lavas (solid dots) plot on an extension of the global MORB trend to low Na Fe, other lavas (open squares) plot in a scattered field consistent with modification by crystal fractionation processes. Vectors depict plagioclase, clinopyroxene, and olivine accumulation. Fields for experimental fertile and depleted mantle melts regressed to MgO = 8 wt.% (Hawaiian pyrolite and Tinaquillo lherzolite, respectively), Lau backarc basin basalt (BABB), and the Tonga-Kermadec arrays (lighter stipple uncorrected for crystal accumulation) are after Turner et al. (1997) and references therein. Global MORB trend is after Pearce et al. (1995).

6. Nb versus Yb for representative Raoul lavas Most form a cluster centered on 25 % melting of a source depleted by 2 % melt extraction relative to FMM (Nb and Yb analyses by ICP-MS). Three lavas plot as outliers. Calibration of the diagram, South Sandwich, Mariana, New Hebrides, and Aleutian fields after Pearce and Parkinson (1993).

7. MORB normalized incompatible element plot for representative Raoul lavas. The analyses bracket the spread of MORB-normalised patterns. Element abundances increase with SiO_2, LILI are enriched and most HFSE are flat. Normalisation factors after Pearce and Parkinson (1993).

8. Behavior of non-conservative incompatible elements in subduction zones. Four distinct trends can be generated by varying the relative inputs of mantle wedge and subducted crust. See text for further discussion.

9. X/Yb versus Nb/Yb (where X is an incompatible element) for representative Raoul lavas (solid diamonds). Fields for South Sandwich (moderate shading data from Pearce and Peate, 1995 Pearce et al., 1995)), Mariana (cross hatching, data from Elliot et al 1997) and Ruapehu (dark shading, data from Price et al., 2005 and references therein) are shown for comparison. The MORB array and average MORB (solid dot) are also shown Dotted lines are contour lines and the amount of a subduction component is shown as a percent.The open headed arrow is an extrapolation of the Raoul array to Nb/Yb values comparable to average MORB.

10. Plot of X/Z (Ba/Rb, Ba/Pb, Ba/Th and Ba/Nb) versus Nb/Yb. Dashed lines are arbitrary ratios of X/Z, double headed arrow is a least squares power curve fitted to the Raoul array. South Sandwich and Mariana arrays are data from Pearce et al. (a995) and Elliot et al. (1997) respectively.

11. Plots of $^{87}/_{86}$Sr and $^{206}/_{204}$Pb versus Nb/Yb models invoking a constant subduction-related component, constant mantle component and a fixed ratio of mixing between these components predict horizontal arrays on both plots..Raoul lavas form an array of negative slope for Sr isotopic ratios which is best explained as resulting from continued minor input from the subduction-related component to the melting column. The array for Pb isotope ratios is horizontal within analytical error. Dashed lines are at arbitrary ratios of $^{87}/_{86}$Sr and $^{206}/_{204}$Pb and the double-headed arrow is a least squares power curve fitted to the Raoul array. The south Sandwich array also exhibits a negative

correlation between $^{87}/_{66}$Sr and Nb/Yb. Data bases the South Sandwich and Mariana arcs are from Pearce et al (1995) and Elliot et al (1997) respectively.

Tables

1. Analyses of selected representative Raoul Volcano lavas in the basalt – andesite compositional range. Aphyric lavas are indicated with an A and total phenocryst proportions are given for the other analyses. Sample numbers refer to material archived in the University of Auckland petrology collection. Analytical methods are given in the appendix.
2. Equations for regressing major elements to MgO = 8 wt.% in Raoul lavas. Each linear regression equation is of the form Y = AX + B, where Y is the weight proportion of the element, A is the slope, X is the MgO content, and B is the intercept. The equations were derived using 13 aphyric lava analyses only. r is the correlation coefficient for the element versus MgO.
3. Subduction-related contribution of selected elements in Raoul and other lavas The average subduction-related contribution for each incompatible element is listed, and for Raoul the range is also given. Ruapehu values are those for the low-SiO_2 end of the Type D array (inferred minimal crustal assimilation). Values of Sr for Raoul are aphyric lavas only, and for South Sandwich lavas are from Pearce et al. (1995).
4. Subduction, backarc extension, and Nb/Yb for Raoul and other arcs. No obvious relationship exists for subduction or backarc extension parameters with Nb/Yb for Raoul and the South Sandwich and Mariana arcs. Subduction rates, backarc extension, and backarc basin widths from Plank and Langmuir (1993), Barker (1995), Fryer (1995), and Parson and Wright (1996). Values of

Nb/Yb for the South Sandwich and Mariana arcs from Pearce et al. (1995) and Elliott et al. (1997).

5. Sediment flux beneath Raoul and other arcs. Sediment subduction fluxes for selected elements beneath Raoul were calculated by the method of Plank and Langmuir (1993), using average compositions for DSDP 595/596 and DSDP 204 (upper 103 m only) taken from Turner et al. (1997) and assuming a density of 1.4 g/cm and H content of 40 wt.%. The South Sandwich flux was calculated from data in Ben Othman et al. (1989), whereas the Mariana flux was taken from Plank and Langmuir (1993).

Figure

Click here to download high resolution image

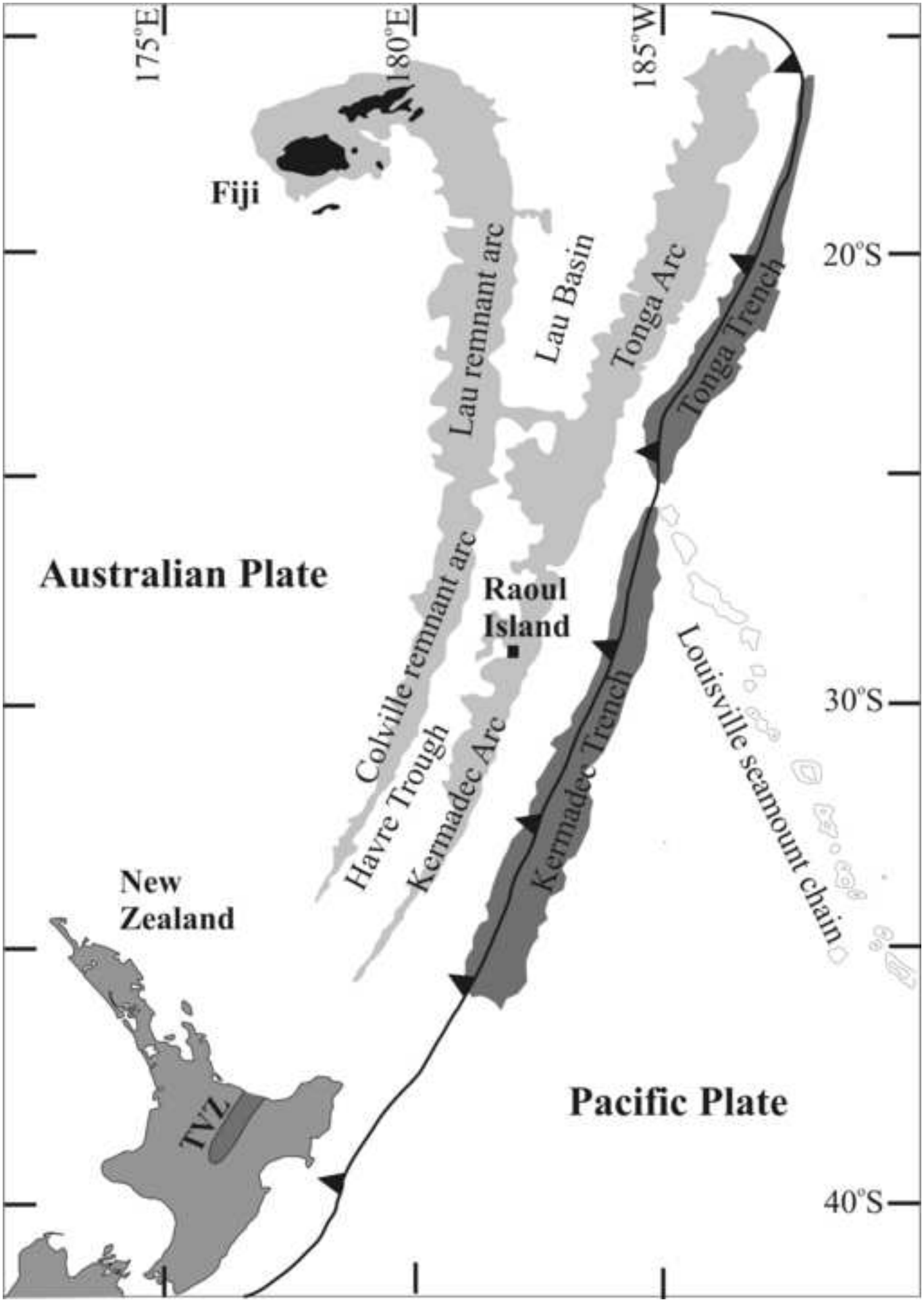

Figure
Click here to download high resolution image

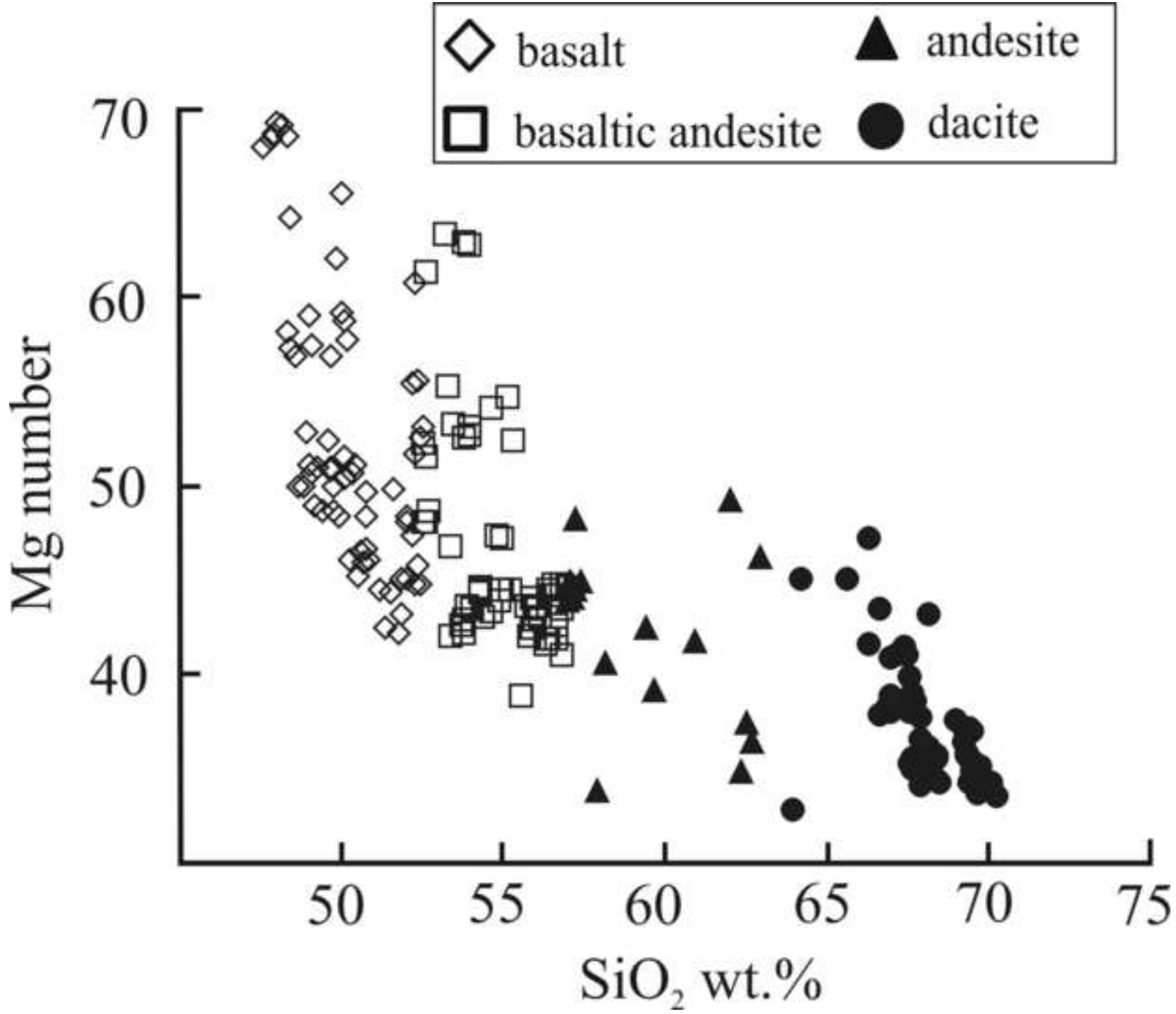

Figure
Click here to download high resolution image

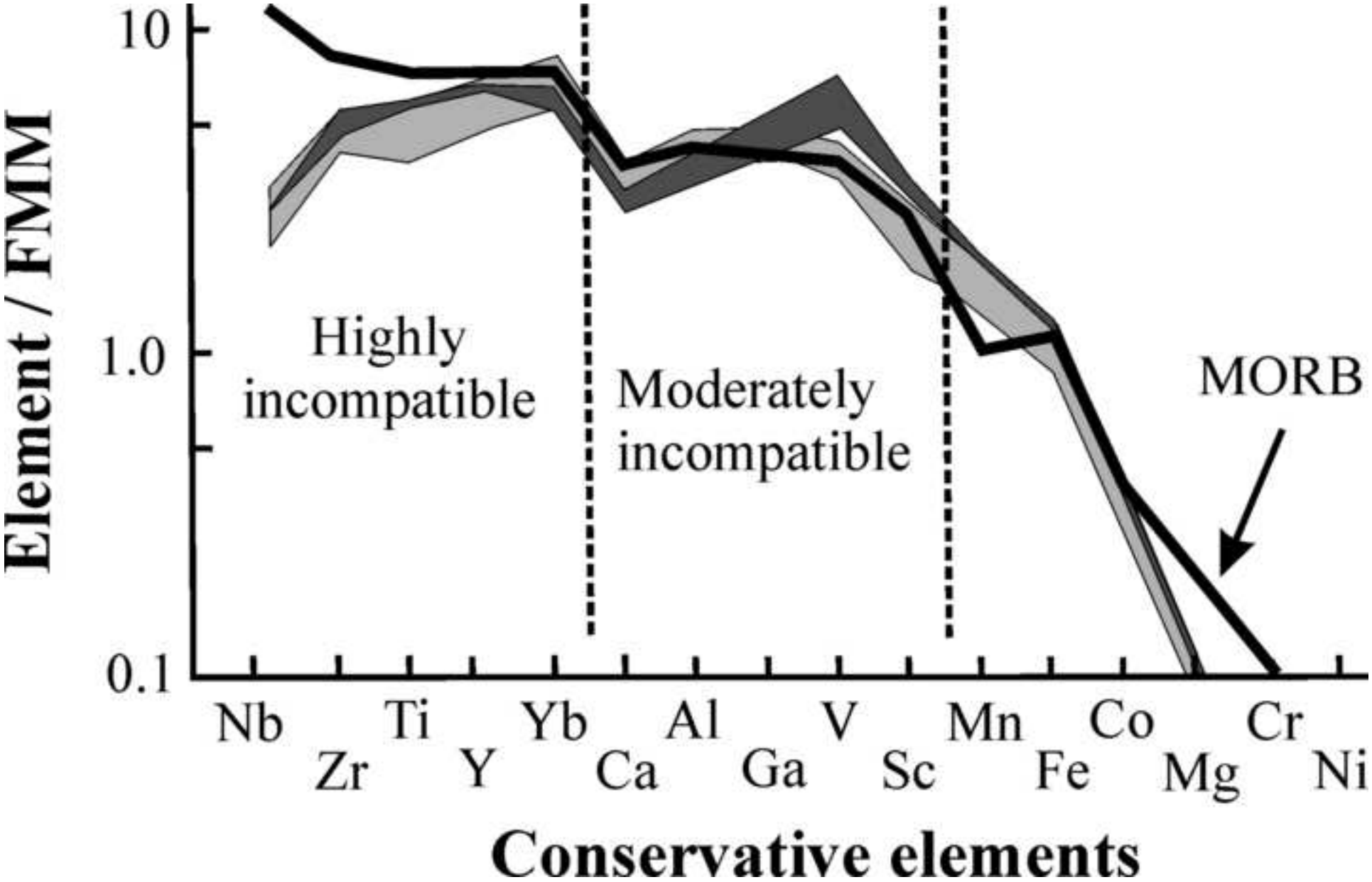

Figure
Click here to download high resolution image

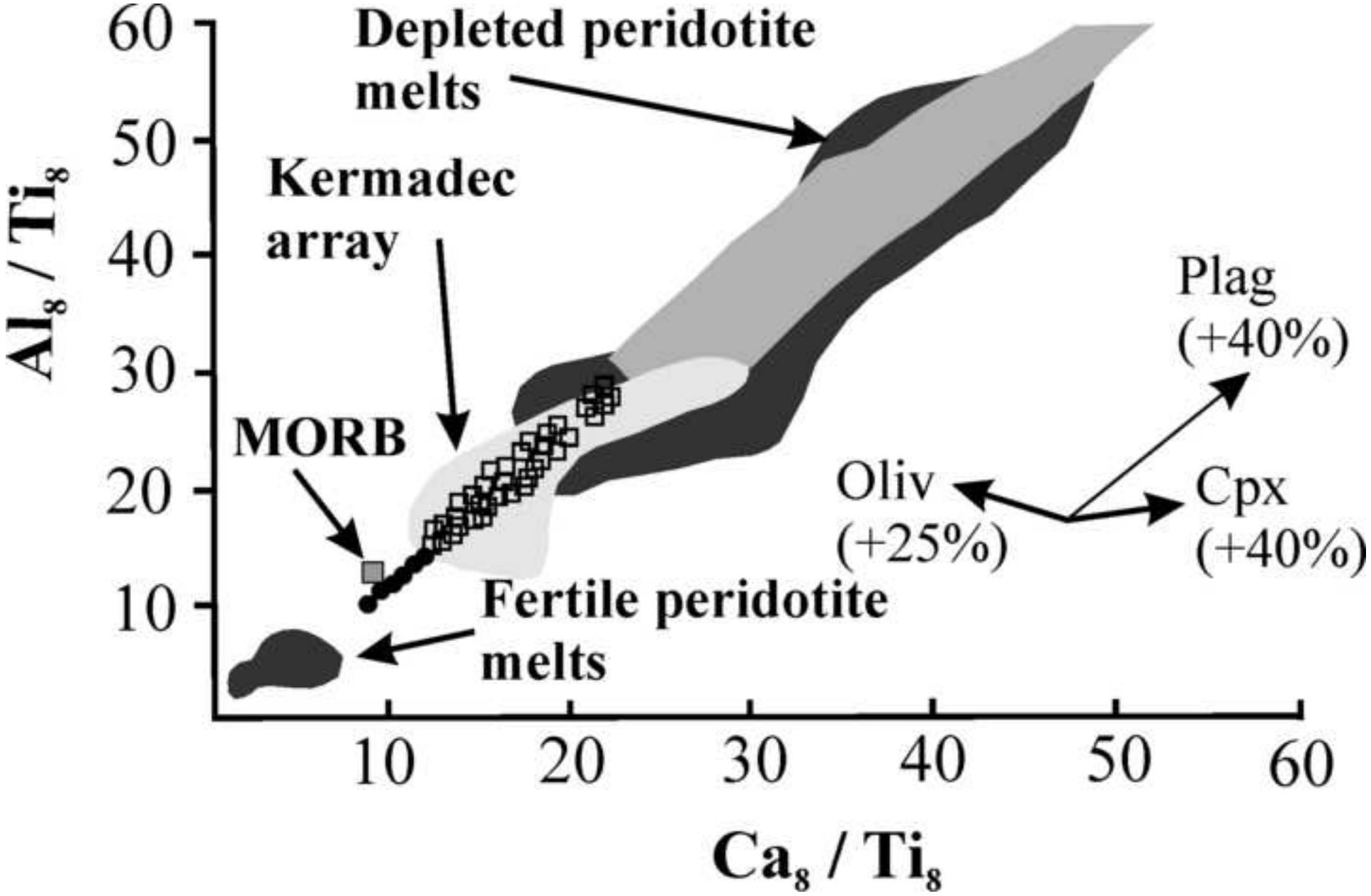

Figure
Click here to download high resolution image

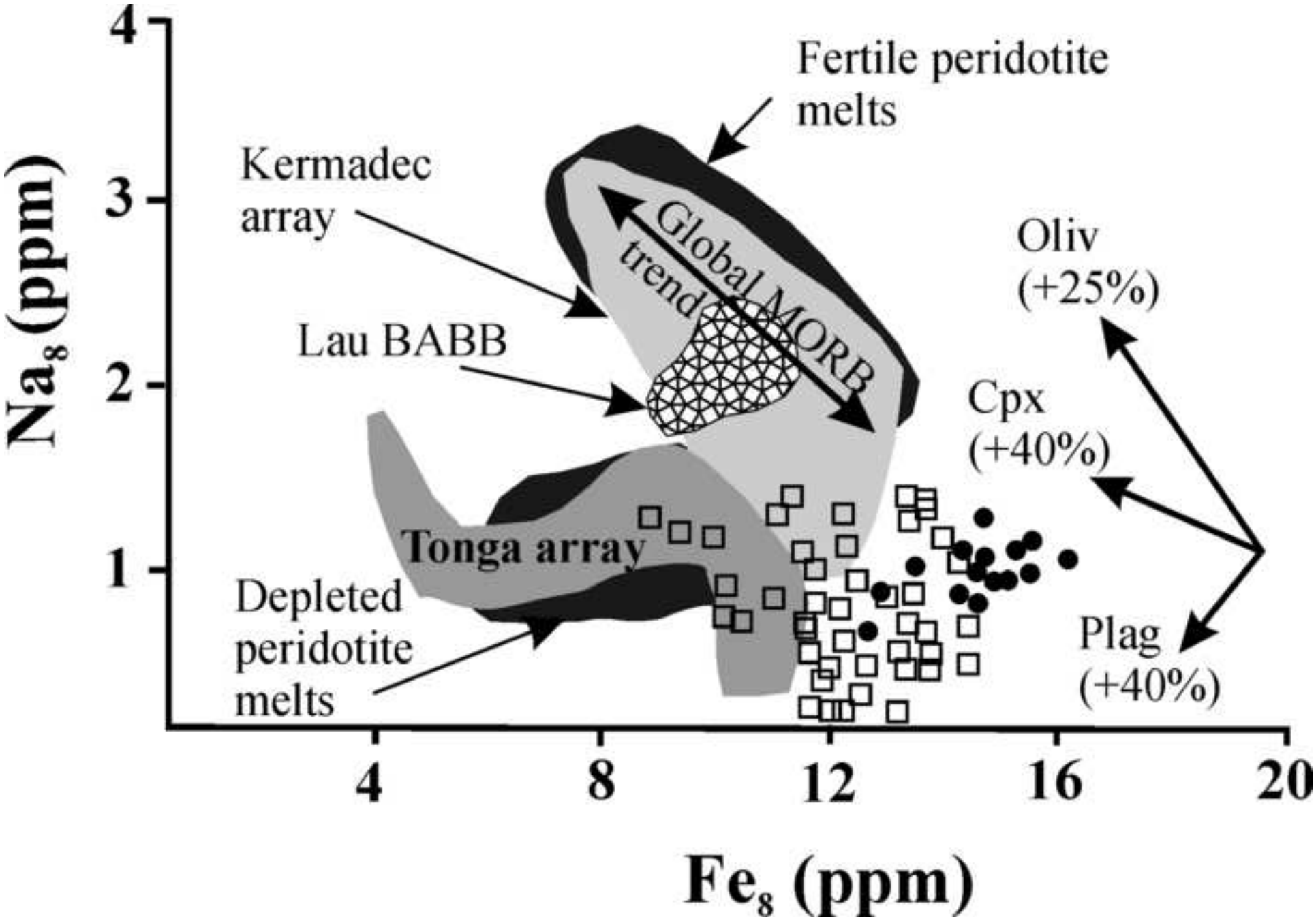

Figure
Click here to download high resolution image

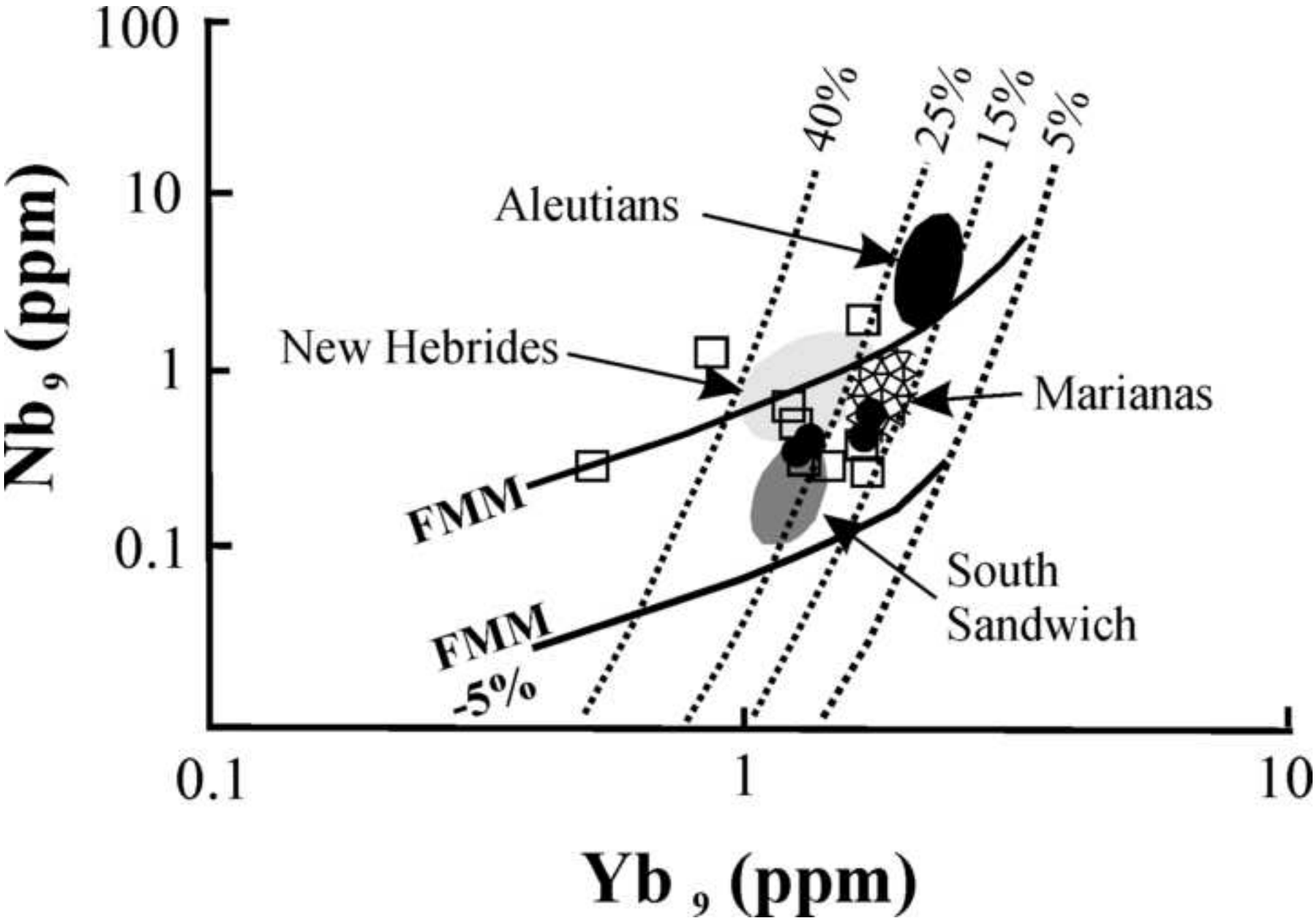

Figure
Click here to download high resolution image

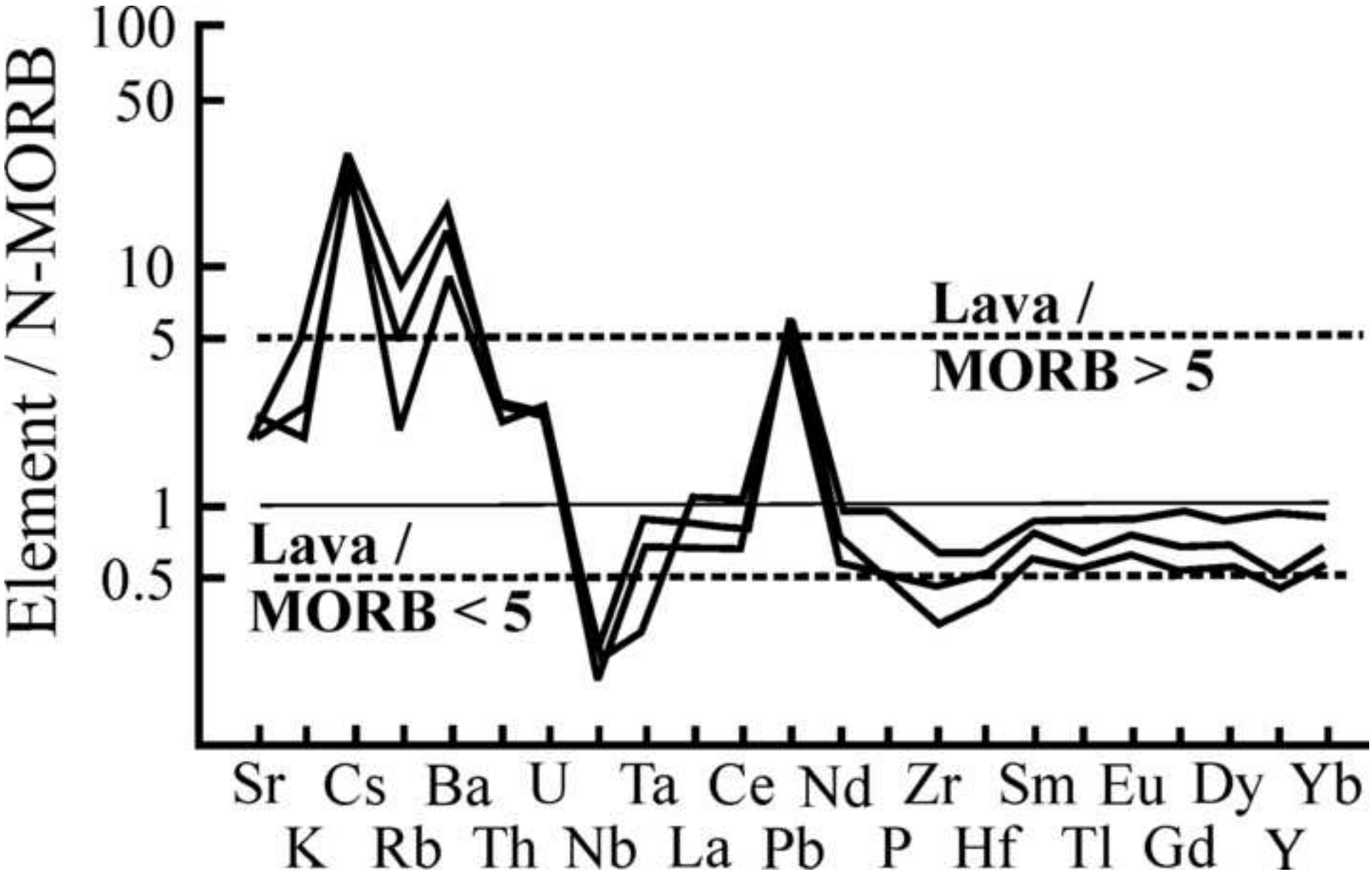

Figure

Click here to download high resolution image

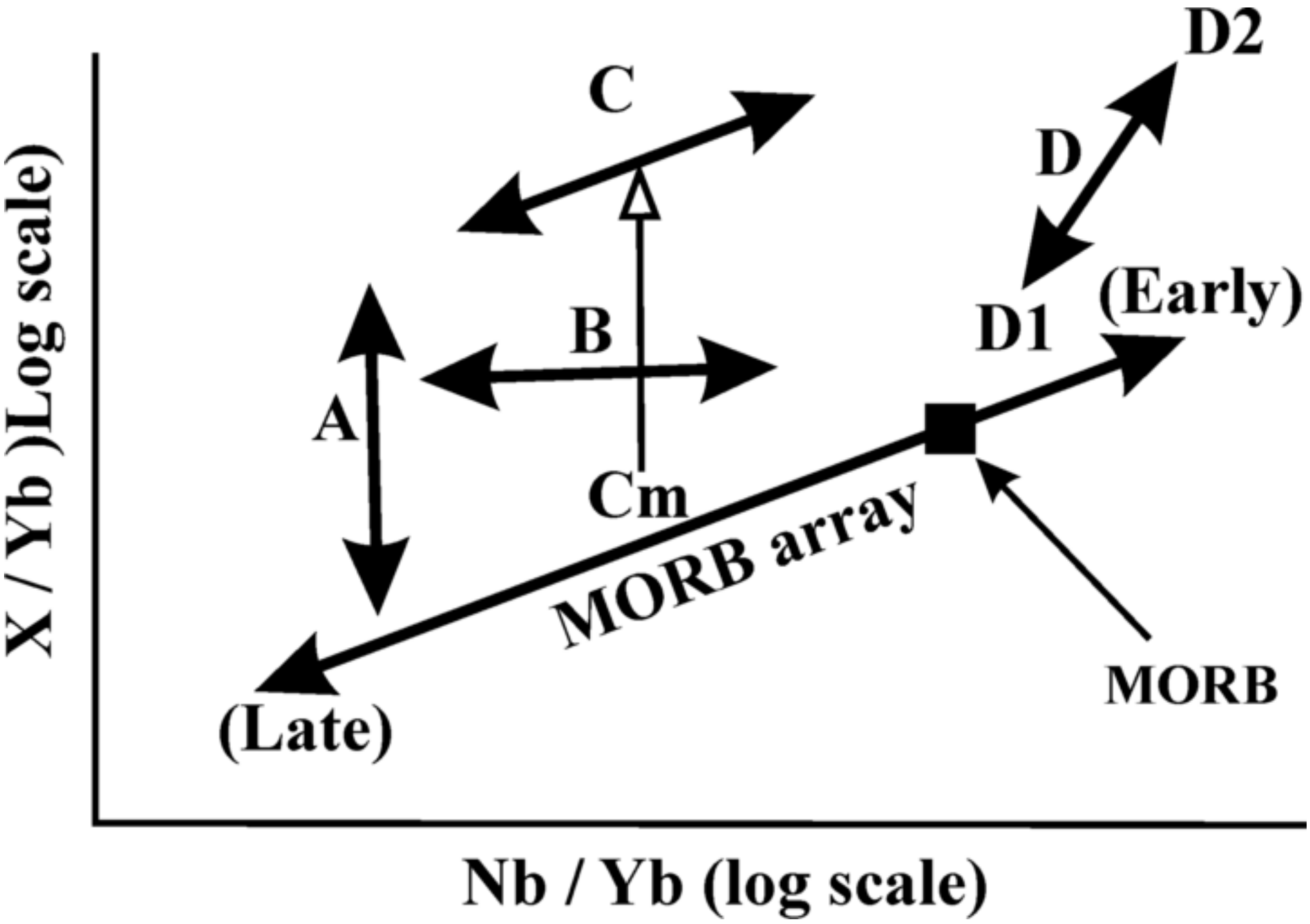

Figure
Click here to download high resolution image

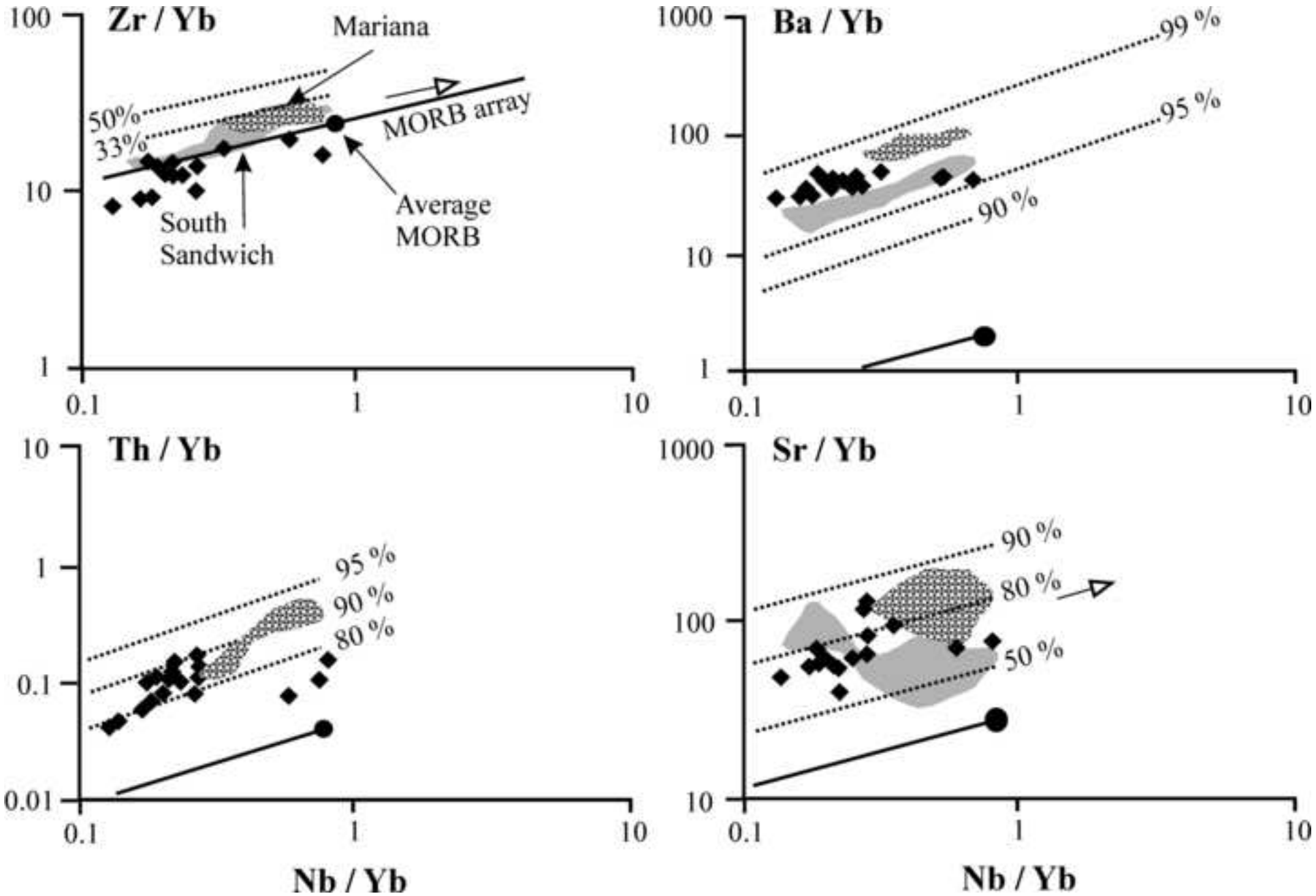

Figure
Click here to download high resolution image

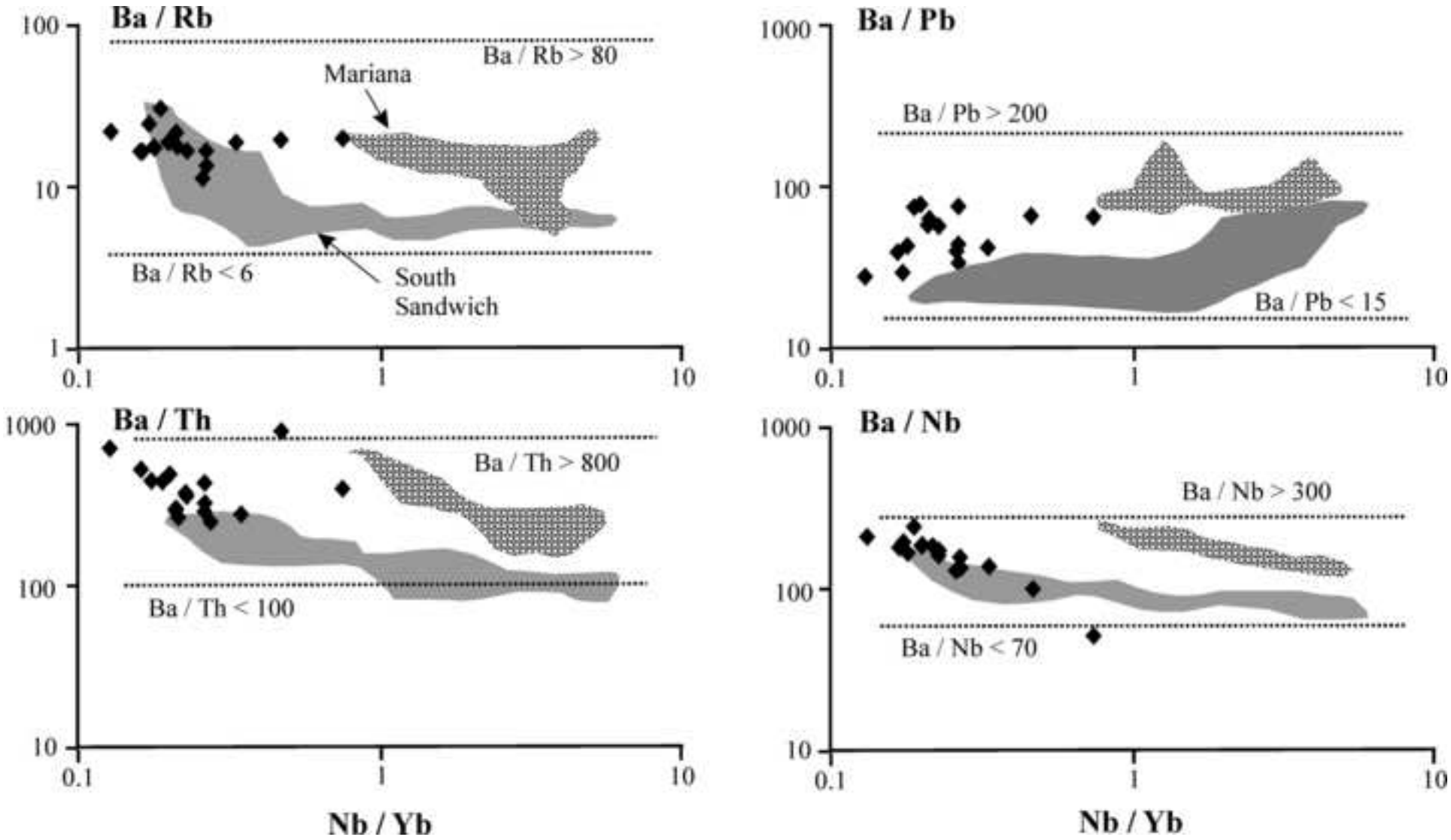

Figure
Click here to download high resolution image

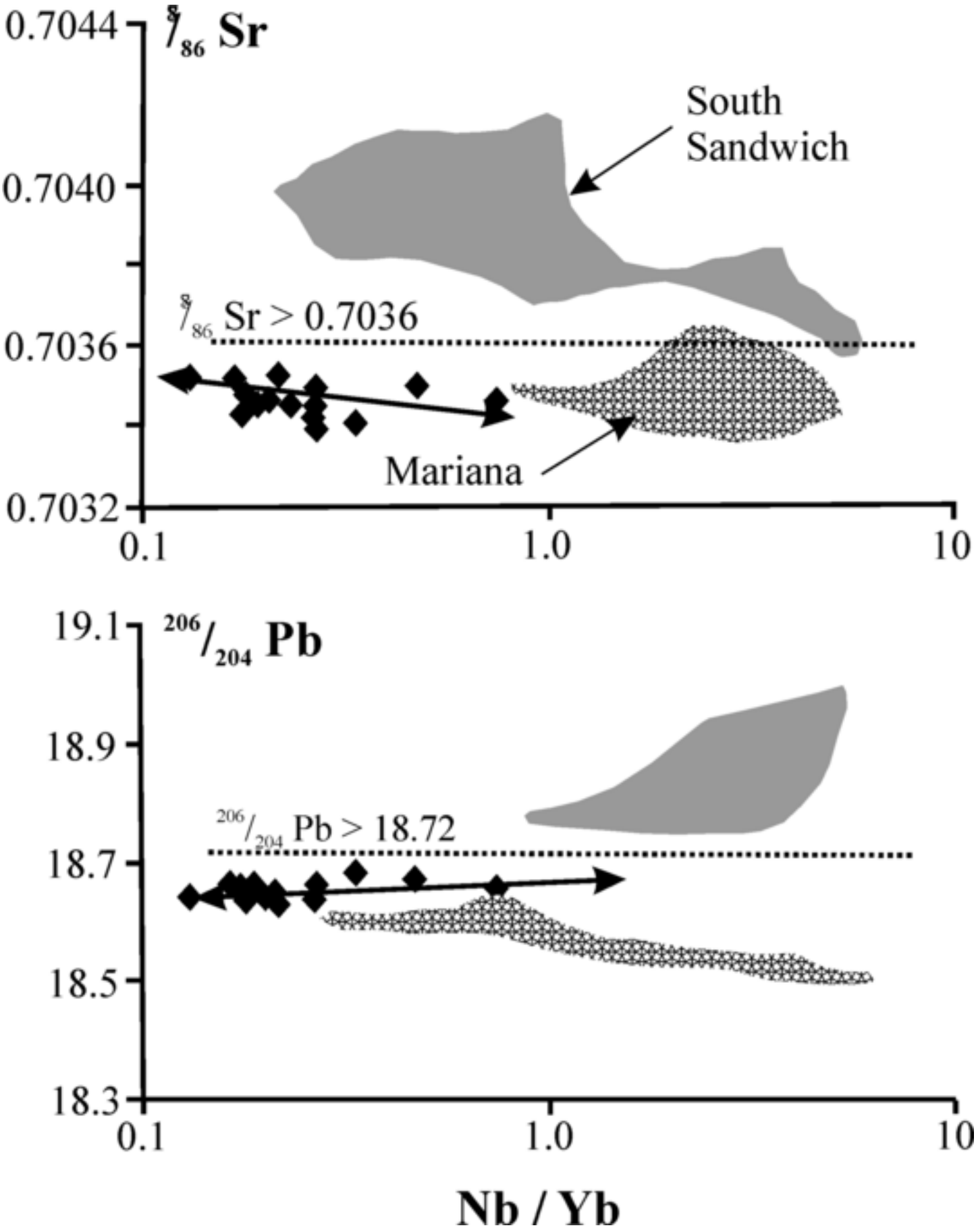

Table

Click here to download Table: table 1.doc

AU No.	7135	7114	46357	7125	46329	46330	7144	46325	7148	7090	7053	7096	46362	46358	46368	7088
	45.4	47.4	36.4	37.0	20.6	27.6	37.4	2.8	22.2	aphyric	3.2	27.6	28.8	9.6	18.0	0.6
wt.%																
SiO_2	47.85	48.84	49.01	49.52	51.44	51.46	51.48	51.67	51.78	53.26	54.83	55.36	55.53	56.50	56.77	57.27
TiO_2	0.56	0.65	0.75	0.72	0.82	0.92	0.76	1.02	0.66	1.01	1.04	0.72	0.71	0.97	0.70	1.23
Al_2O_3	15.55	20.83	19.17	17.69	18.03	17.28	18.52	15.34	17.72	15.15	14.79	18.10	18.20	15.81	17.53	14.10
Fe2O3	1.69	1.58	1.73	1.62	1.76	2.02	1.66	2.17	1.67	2.12	2.09	1.47	1.47	1.81	1.46	2.03
FeO	8.45	7.92	8.63	8.08	8.79	10.11	8.31	10.87	8.36	10.59	10.43	7.35	7.34	9.07	7.31	10.15
MnO	0.18	0.20	0.18	0.19	0.19	0.24	0.19	0.23	0.18	0.25	0.24	0.17	0.18	0.22	0.18	0.23
MgO	10.30	4.61	4.82	6.43	4.61	4.31	4.42	4.95	5.17	4.60	3.72	3.11	3.24	3.55	3.29	2.93
CaO	13.33	12.82	12.18	12.97	11.12	10.45	10.40	10.29	11.22	9.32	8.57	10.18	10.23	8.41	9.59	7.52
Na_2O	0.93	1.47	1.60	1.31	1.79	1.90	1.76	1.80	1.71	2.07	2.50	2.08	2.07	2.50	2.04	2.69
K_2O	0.11	0.14	0.25	0.18	0.28	0.42	0.13	0.33	0.21	0.34	0.41	0.27	0.26	0.47	0.26	0.62
P_2O_5	0.05	0.06	0.09	0.06	0.10	0.13	0.07	0.10	0.06	0.09	0.11	0.08	0.08	0.14	0.08	0.19
H_2O^-	0.03	0.03	0.21	0.06	0.12	0.06	0.68	0.10	0.21	0.06	0.22	0.04	0.10	0.06	0.08	0.18
LOI	0.94	0.88	0.96	0.90	0.98	1.13	0.93	1.21	0.93	1.18	1.16	0.82	0.82	1.01	0.81	1.13
Total	99.97	100.04	99.58	99.72	100.03	100.43	99.31	100.09	99.88	100.04	100.11	99.75	100.22	100.52	100.11	100.27
ppm																
Cs	0.11	0.19	0.23	0.19	0.25	0.25	0.14	0.20	0.11	0.30	0.27	0.30	0.36	0.43	0.16	0.36
Ba	49.0	64.3	109.4	85.3	119.6	113.9	139.4	95.4	81.9	102.7	115.6	108.8	104.2	133.8	106.8	168.4
Sr	151.5	209.0	207.0	161.6	216.2	162.7	171.0	141.7	161.9	149.1	161.8	194.2	184.6	186.5	172.6	160.0
Pb	1.21	1.89	2.59	1.95	1.87	1.50	1.91	1.66	2.75	1.76	1.49	2.57	2.58	1.30	3.78	2.71
Th	0.10	0.18	0.37	0.26	0.29	0.41	0.29	0.30	0.22	0.24	0.22	0.22	0.19	0.19	0.15	0.58
U	0.10	0.11	0.17	0.10	0.16	0.11	0.16	0.10	0.10	0.11	0.12	0.14	0.16	n/a	0.18	0.18
Zr	12.7	21.9	37.9	26.0	43.0	34.1	37.4	30.7	33.1	28.4	34.4	30.2	29.0	49.8	28.9	55.7
Nb	0.32	0.42	0.70	0.50	1.99	0.64	0.52	0.53	0.39	0.54	0.55	0.58	0.53	1.42	0.46	0.83
Hf	0.45	0.77	1.55	0.96	1.49	1.32	1.55	1.20	1.39	1.45	1.46	1.33	1.29	1.27	1.22	2.51
Ta	0.16	0.08	0.20	0.11	0.27	0.03	0.13	0.04	0.08	0.04	0.03	0.17	0.09	n/a	0.10	0.06
Y	10.0	12.0	17.3	14.8	24.5	19.3	22.2	20.0	18.1	19.4	21.2	24.7	22.8	25.9	25.3	32.3

Sc	52.6	35.3	36.3	42.9	41.7	31.9	38.9	39.1	40.6	35.8	35.0	33.2	31.4	35.9	32.5	30.9
V	352.7	377.6	350.1	346.8	351.4	335.7	344.2	424.0	334.4	461.4	365.8	307.3	296.5	301.5	279.1	268.2
Cr	227.6	17.5	45.6	137.7	40.2	12.0	28.4	19.6	25.6	17.8	24.0	15.7	18.1	15.4	16.6	5.8
Co	54.4	35.4	42.6	40.2	40.2	32.9	34.6	34.1	38.3	31.8	27.3	29.0	27.9	26.1	27.2	25.3
Ni	97.9	25.3	36.8	58.3	33.9	19.1	23.9	17.7	28.4	17.8	16.6	20.2	19.3	13.1	19.7	7.4
Cu	73.4	81.2	147.5	84.3	140.1	96.6	102.2	178.6	143.8	142.1	113.1	140.8	74.4	86.1	64.6	102.2
Zn	50.5	55.8	66.3	59.7	67.9	65.1	66.2	67.1	60.8	68.1	73.6	67.8	66.1	76.2	67.3	81.5
Ga	10.6	13.6	14.3	12.7	18.1	12.2	13.6	11.6	12.9	11.9	12.4	13.9	13.7	16.1	13.5	13.1
Ge	0.45	0.44	0.69	0.80	0.91	0.60	0.57	0.57	0.57	0.60	0.59	0.60	0.57	1.13	0.54	0.81
La	1.29	1.54	3.31	1.96	3.07	3.25	2.34	2.49	1.70	2.35	2.71	2.60	2.61	2.65	2.48	4.54
Ce	3.85	4.53	9.03	5.66	8.68	8.71	6.33	7.00	5.18	6.69	7.66	7.75	7.61	7.52	7.34	11.99
Pr	0.68	0.80	1.46	0.97	1.47	1.47	1.25	1.18	0.92	1.17	1.34	1.41	1.36	1.17	1.34	2.11
Nd	3.34	4.11	7.48	5.07	7.72	7.70	6.44	6.26	5.08	5.98	6.95	7.28	7.35	6.95	7.55	11.26
Sm	1.27	1.44	2.54	1.76	2.63	2.46	2.41	2.17	1.82	2.21	2.50	2.77	2.73	2.21	2.75	3.81
Eu	0.48	0.57	0.93	0.70	1.02	0.87	0.91	0.81	0.73	0.88	0.98	0.99	1.10	0.82	1.07	1.28
Gd	1.51	1.76	2.84	2.30	3.45	3.13	3.18	3.05	2.60	3.05	3.12	3.56	3.35	2.86	3.67	5.11
Tb	0.27	0.33	0.51	0.40	0.60	0.51	0.52	0.46	0.42	0.41	0.52	0.68	0.71	0.56	0.70	0.74
Dy	1.89	2.28	3.22	2.85	3.96	3.49	3.84	3.41	3.07	3.08	3.98	4.72	4.60	3.99	4.80	5.35
Ho	0.42	0.49	0.73	0.59	0.91	0.79	0.84	0.77	0.70	0.72	0.92	1.02	0.99	0.80	1.08	1.27
Er	1.13	1.48	1.98	1.58	2.31	2.05	2.25	2.07	1.85	1.89	2.41	2.86	2.78	2.15	3.02	3.19
Tm	0.18	0.22	0.31	0.25	0.42	0.38	0.41	0.39	0.32	0.38	0.41	0.45	0.40	0.40	0.41	0.67
Yb	1.24	1.57	2.11	1.87	2.67	2.41	2.74	2.51	2.25	2.32	2.76	3.24	3.18	2.53	3.53	3.87
Lu	0.16	0.20	0.33	0.22	0.41	0.34	0.34	0.33	0.29	0.37	0.38	0.44	0.45	0.39	0.48	0.55
$^{87}Sr/^{86}Sr$	0.70342	0.70349	0.70341	0.70340	0.70347	0.70345	0.70346	0.70353	0.70343	0.70345	0.70346	0.70347	0.70352	0.70349	0.70352	0.70353
$^{143}Nd/^{144}Nd$	0.51306	0.51305	0.51303	0.51305	0.51304	0.51304	0.51305	0.51305	0.51305	0.51304	0.51304	0.51305	0.51307	0.51305	0.51305	0.51303
$^{206}Pb/^{204}Pb$	18.648	18.662	18.685	18.639	18.652	18.656	18.656	18.647	18.659		18.643	18.646	18.667	18.656	18.641	18.636
$^{207}Pb/^{204}Pb$	15.571	15.558	15.577	15.563	15.566	15.556	15.565	15.555	15.571		15.546	15.556	15.574	15.559	15.565	15.555
$^{208}Pb/^{204}Pb$	38.342	38.316	38.371	38.343	38.333	38.305	38.316	38.286	38.387		38.268	38.332	38.356	38.320	38.319	38.288

Table

Click here to download Table: Table 2.doc

Element vs. MgO	Slope	Intercept	r^2
SiO_2	-3.216	68.866	0.86
TiO_2	0.043	0.863	0.05
Al_2O_3	0.12	14.399	0.06
FeO	1.13	5.692	0.57
CaO	1.109	4.285	0.92
Na_2O	-0.341	3.696	0.81
K_2O	-0.058	0.652	0.21

Table

Click here to download Table: Table 3.doc

	Raoul		South Sandwich	Mariana	Ruapehu
Element	range	average	average	average	(basalt)
Zr	<20%	5%	10%	25%	5%
Nd	20-40%	30%	30%	40%	35%
La	50-60 %	55%	55%	65%	55%
Sr	70-80 %	75%	80%	82%	65%
Th	80-90 %	85%	90%	90%	90%
K	80-95 %	90%	87%	92%	80%
Pb	91-97 %	95%	95%	92%	92%
Rb	95-97 %	96%	96%	96%	96%
Ba	96-98%	98%	96%	98%	96%
Cs	99->99%	99%	99%	99%	98%

Table

Click here to download Table: Table 4.doc

	Subduction cm/year	Backarc extension cm/year	Basin width km	Nb/Yb range	Nb/Yb average
Raoul	8.1	2.1	130	0.13-0.33	0.22
South Sandwich	7.5	6.5	250	0.14-0.76	0.34
Central Mariana	7.7	3	240	0.28-0.72	0.49

Table

Click here to download Table: Table 5.doc

	Raoul		South Sandwich	Mariana
Subduction cm/yr)	8.1		7.5	7.7
Crust (age)	Jurassic		27-80 Ma	Jurassic
Sediment (m)	100-150		200-400	300-500
Data source:	DSDP595/596	DSDP204		
Ba (g/yr/arc-cm)	145	38	95	140
Rb(g/yr/arc-cm)	3.4	5.3	7.6	12.1
Th (g/yr/arc-cm)	0.84	0.73	0.69	1.02
K(g/yr/arc-cm)	1490	2130	1990	3610
Sr (g/yr/arc-cm)	20	16	44	35
La (g/yr/arc-cm)	11.4	5.4	1.7	6.2
87Sr/86Sr	0.7095	0.7075	0.7087	0.7062
206Pb/204Pb	18.76	18.81	18.64	18.92